Inhibition of PI3Kinase-α is pro-arrhythmic and associated with enhanced late Na^+ current, contractility, and Ca^{2+} release in murine hearts

Short Title: PI3Kα inhibition and arrhythmias

Authors: Pavel Zhabyeyev,[1,3] PhD, Brent McLean,[1,2,3] PhD, Xueyi Chen,[1,3] MD, Bart Vanhaesebroeck,[4] PhD, Gavin Y. Oudit,[1,3,] * MD, PhD

Affiliations: [1]Department of Medicine, University of Alberta, Edmonton, Canada
[2]Department of Physiology, University of Alberta, Edmonton, Canada
[3]Mazankowski Alberta Heart Institute, University of Alberta, Edmonton, Canada
[4]UCL Cancer Institute, London, UK

Corresponding Author: *Gavin Y. Oudit, MD, PhD, FRCPC
Division of Cardiology, Department of Medicine
8440 112 Street NW
Edmonton, AB, T6G 2B7
Canada
Phone: 780 407 8569
Fax: 780 407 6452
Email: gavin.oudit@ualberta.ca

Word Count: 8932 words (total), 5502 words (text); 8 Figures, 1 Supplemental table, 7 Supplemental Figures, and 2 Supplemental Videos)

CONFLICT OF INTEREST:

Pavel Zhabyeyev	NONE
Brent McLean	NONE
Xueyi Chen	NONE
Bart Vanhaesebroeck	NONE
Gavin Y. Oudit	NONE

Abstract

Background: Phosphoinositide 3-kinase α (PI3Kα) is a proto-oncogene with high activity in the heart. BYL719 (BYL) is a PI3Kα-selective small molecule inhibitor and a prospective drug for advanced solid tumors. We investigated whether acute pharmacological inhibition of PI3Kα has pro-arrhythmic effects.

Methods & Results: In isolated wild-type (WT) cardiomyocytes, pharmacological inhibition of PI3Kα (BYL719) increased contractility by 28%, Ca^{2+} release by 20%, and prolonged action potential (AP) repolarization by 10-15%. These effects of BYL719 were abolished by inhibition of reverse-mode Na^+/Ca^{2+} exchanger (NCX) (KB-R7943) or by inhibition of late Na^+ current (I_{Na-L}) (ranolazine). BYL719 had no effect on PI3Kα-deficient cardiomyocytes, suggesting BYL719 effects were PI3Kα-dependent and mediated *via* NCX and I_{Na-L}. I_{Na-L} was suppressed by activation of PI3Kα, application of exogenous intracellular PIP3, or ranolazine. Investigation of AP and Ca^{2+} release in whole heart preparations using epicardial optical mapping showed that inhibition of PI3Kα similarly led to prolongation of AP and enhancement of Ca^{2+} release. In hearts of PI3Kα-deficient mice, β-adrenergic stimulation in the presence of high Ca^{2+} concentrations and 12-Hz burst pacing led to delayed afterdepolarizations and ventricular fibrillation. In vivo, administration of BYL719 prolonged QT interval [QT_{cF} (Fridericia) increased by 15%] in WT, but not in PI3Kα-deficient mice.

Conclusions: Pharmacological inhibition of PI3Kα is arrhythmogenic due to activation of I_{Na-L} leading to increased sarcoplasmic reticulum Ca^{2+} load and prolonged QT interval. Therefore, monitoring of cardiac electrical activity in patients receiving PI3K inhibitors may provide further insights into the arrhythmogenic potential of PI3Kα inhibition.

Key Words: PI3Kα, arrhythmias, long QT, afterdepolarization, adrenergic stimulation

1. Introduction

Phosphoinositide 3-kinase (PI3K) consists of the p110α catalytic subunit of PI3Kα (encoded by *PIK3CA* gene) and a p85 regulatory subunit. The kinase is activated by receptor tyrosine kinase (TK) and modulates cell survival, growth, metabolism, and myocardial contractility *via* production of phosphatidylinositols (PtdIns) (3,4,5)P3 (PIP3) [1-3]. Upregulation of PI3K signaling due to gain-of-function mutations in the *PIK3CA* gene is common in many cancers, making the PI3Kα pathway a target for new cancer drugs [2, 4, 5]. A number of clinical trials are in progress to test specific PI3Kα inhibitors (*e.g.*, taselisib, GDC0032 [6]; alpelisib, BYL719 [7, 8]; TAK117, MLN1117 [9]), pan-PI3K inhibitors (*e.g.*, BKM120 [10]), and tyrosine kinase inhibitors that inhibit PI3Kα activity [11] (*e.g.*, ibrutinib [12]). Inhibition of PI3K and/or TK activity is known to adversely impact the heart as such inhibitors had been linked to cardiotoxicity and heart failure [2, 4]. Arrhythmogenic side effects have been reported for copanlisib and ibrutinib [5, 11]. Copanlisib, a novel pan-PI3K inhibitor, prolonged QT_c ($\Delta QT_{cB} \geq 60$ ms) in up to 6.6% patients, which resulted in a request for further monitoring by the FDA [5]. Ibrutinib increased instances of a cardiac disorder and atrial fibrillation by 2- and 3-fold, respectively, in comparison to the anti-CD20 monoclonal antibody ofatumumab [12]. Besides that, ibrutinib is linked to ventricular arrhythmias and sudden cardiac death in patients [13, 14]. A link between PI3Kα activity and arrhythmias has been observed not only for cancer drugs but also for diabetes, which also lowers PI3Kα activity [15, 16]. Diabetes mellitus is known to be associated with a prolonged QT interval, which was linked to activation of late Na^+ current ($I_{Na\text{-}L}$) due to a lack of PI3Kα activity [15, 16]. Conversely, upregulation of PI3Kα activity in the heart protects it

from ventricular arrhythmias and sudden death associated with pathological hypertrophy and heart failure [17, 18].

Arrhythmogenic activation of I_{Na-L} secondary to PI3Kα inhibition was also shown for some classical blockers of rapidly activating delayed rectifier K^+-channels (I_{Kr} blockers), such as dofetilide and E4031 [19]. In addition, gain-of-function mutations in genes encoding Na^+ channels (*SCN5A* and *SCN10*) are involved in the development of heart failure in a rodent model [20] and associated with dilated cardiomyopathy [21] as well as arrhythmias, including sudden cardiac death [22, 23]. This growing body of evidence linking PI3Kα inhibition, I_{Na-L}, and arrhythmogenic phenomena necessitates a rigorous examination of the underlying mechanisms and rigorous testing of new generation PI3K inhibitors. Our preliminary report showed that PI3Kα inhibition results in enhanced contractility and Ca^{2+} release accompanied by prolongation of an action potential (AP) and QT interval [24]. Most of the previous studies on the link between inhibition of PI3K signaling and arrhythmogenic consequences such as long-QT (LQT) syndrome and atrial fibrillation [11, 19, 25] were mainly based on non-specific PI3K inhibitors and were limited to isolated cardiomyocytes. The specific PI3Kα inhibitor (BYL719) increased I_{Na-L} and triggered activity in cardiomyocytes [26]. However, no previous studies performed ex vivo and in vivo studies or considered the involvement of Ca^{2+} cycling or possible interplay with β-adrenergic stimulation, both of which are important contributors to the development of several arrhythmias [23, 27].

In this study, we used a specific inhibitor of PI3Kα (BYL719) and mice with cardiomyocyte-specific PI3Kα deficiency (p110$\alpha^{f/f}$-Cre) to elucidate the consequence of specific PI3Kα inhibition at the cellular, organ, and animal levels. First, our work confirmed that PI3Kα

inhibition is inherently pro-arrhythmic (associated with QT prolongation and triggered activity). Second, we demonstrated that the inhibition is associated with increased Ca^{2+} load of sarcoplasmic reticulum (increased caffeine-induced Ca^{2+} release, Ca^{2+} transients, and myocyte contractility). Thirdly, the effects of PI3Kα inhibition are additive with β-adrenergic stimulation. Lastly, we found that the effects of PI3Kα inhibition can be mitigated by a late Na^+ current blocker (e.g., ranolazine) and/or reverse-mode Na^+-Ca^{2+} exchanger blocker.

2. Methods

2.1. Experimental animals.

At 10-12 weeks of age, C57BL/6J male mice [wild type (n=57), p110$\alpha^{flx/flx}$ (p110$\alpha^{f/f}$, n=24), and αMHC-Cre-p110$\alpha^{flx/flx}$ (p110$\alpha^{f/f}$-Cre, n=20)] were studied. Transgenic mice, p110$\alpha^{f/f}$-Cre, were obtained by cross-breeding mice with constitutively active Cre recombinase under the control of the αMHC promoter and mice carrying PI3Kα gene (*PIK3CA*) flanked with loxP sites, as previously described [28]. Hearts were excised under anesthesia (2% isoflurane) and were either used for whole-heart perfusions or isolations of cardiomyocytes as previously described [29]. Electrocardiographic recordings (ECG) were performed in anesthetized mice (1.5% isoflurane). All animals received care according to the standards of the Canadian Council of Animal Care, and all procedures were approved by the University of Alberta Health Sciences Animal Welfare Committee. All procedures were compliant with the Guidelines for the Care and Use of Laboratory Animals published by the US National Institutes of Health (NIH Publication, 8th Edition, 2011; University of Alberta assurance number: A5070-01).

2.2. Isolation and culture of cardiomyocytes.

Myocytes were isolated as described previously [29]. After isolation, myocytes were kept in perfusion buffer solution (pH 7.4) and used for contractility or patch-clamp measurements, loading with FURA-2AM or FURA-4F-AM for Ca^{2+} measurements, or plating for myocyte culture. Isolated cardiomyocytes were cultured as described previously [29] with plating buffer containing 25 µmol/l (–)-blebbistatin (Sigma-Aldrich, Canada). After Ca^{2+} reintroduction and plating in media containing 10% serum, cardiomyocytes were cultured in serum-free media with ITS supplement (Sigma Aldrich, Canada) for 30 min before the introduction of 0.2% fetal bovine serum supplemented with 50 U/L (1.74 mg/l) insulin and the addition of 100 nmol/l BYL. BYL was added from a stock solution of 10 mmol/l in dimethyl sulfoxide (DMSO), stored frozen at –20 °C.

2.3. Single cardiomyocyte contractility.

Myocytes were superfused with modified Tyrode's solution (containing in mmol/l: 135 NaCl, 5.4 KCl, 1.2 $CaCl_2$, 1 $MgCl_2$, 1 NaH_2PO_4, 10 Taurine, 10 HEPES, 10 glucose; pH 7.4 with NaOH) at 35-36°C and paced with field stimulation at 1 Hz. Sarcomere length was calculated in real time by software (900B VSL, Aurora Scientific, Canada) from images captured by a high-speed camera at the rate of 200 s^{-1}. Myocytes producing contraction of stable amplitude and kinetics at steady state were selected for analysis. Measurements of fractional shortening, –

dL/dt (rate of contraction, C), and +dL/dt (rate of relaxation, R) were done at steady state (after 2 min of continuous stimulation).

2.4. Ca^{2+} transients and caffeine spurts in isolated myocytes.

Ca^{2+} transients. Myocytes were loaded with membrane-permeable Ca^{2+} sensitive dye [1 µM FURA-2AM (ThermoFisher Scientific, Canada) in Ca^{2+}-free Tyrode's solution] for 15 min at 35-36 °C. After that, myocytes were incubated in Ca^{2+}-free modified Tyrode's solution for 15 min at 35-36 °C and stored later at room temperature protected from light. Aliquots of the solution containing myocytes were placed in a bath mounted on top of an inverted microscope (Olympus IX71, Olympus, Canada) connected to a spectrofluorometer (RatioMaster, Photon Technology International, Inc., USA). Myocytes were superfused with modified Tyrode's solution (same as for contractility measurements) containing 1.2 mM Ca^{2+} at 35-36 °C and paced with field stimulation at 1 Hz (stimulator Grass S48, Astro-Med Inc., USA). Ca^{2+} transients were recorded at emission frequency 510 nm using two excitation frequencies (340 nm and 380 nm) at 200 cycles/s. Transients for the final 40 s of 1 min stimulation were consequently averaged to reduce the noise. The ratio of the signal at 340 nm to the signal at 480 nm was used to calculate the amplitude of Ca^{2+} release [the difference between peak (systolic Ca^{2+} levels) and trough (diastolic Ca^{2+} levels)] and time constant of the Ca^{2+} transient.

Caffeine spurts. Myocytes were loaded with membrane-permeable Ca^{2+} sensitive dye [2 µM FURA-4F-AM (ThermoFisher Scientific, Canada) in Ca^{2+}-free Tyrode's solution] the same way as for Ca^{2+} transients. FURA-4F fluorescence was measured in the same experimental

equipment using the same solutions (1.2 mM Ca^{2+}) at 35-36 °C and the same excitation/emission wavelengths at 200 cycles/s. Maximal Ca^{2+} release was invoked in quiescent myocytes by application of 20 mM caffeine via custom-built rapid-application perfusion system. The opening of the wide pipet was placed near the myocyte (<100 μm away) using a micromanipulator to ensure rapid application of caffeine. The signal was filtered by the adjusted averaging algorithm with the window size of 17 data points. The resulting trace was used to calculate the diastolic Ca^{2+} level and maximal Ca^{2+} level. Maximal Ca^{2+} release was reported as a difference between maximal Ca^{2+} level and diastolic Ca^{2+} level.

2.5. Patch-clamp recordings.

Aliquots of the solution containing myocytes were placed in a bath mounted on top of an inverted microscope (Olympus IX71, Olympus, Canada), and rod-shaped quiescent myocytes were selected for the study. Myocytes were superfused with modified Tyrode's solution (same as for contractility measurements) at 35-36 °C. Pipettes with a resistance of 1.5-2.5 MOhm filled with either K^+ pipette solution (used for measurement of action potential and K^+ currents) or Cs^+ solution (used for measurement of Ca^{2+} and late-Na^+ currents) were zeroed in the solution, then used to form a tight seal, and after that the membrane under the pipette was ruptured using the zap function of the amplifier and gentle suction. Current and membrane potential was measured using a Multiclamp 700B amplifier (Molecular Devices, USA) in voltage or current-clamp mode, respectively. Measured signal was digitized at 10 kHz by 16-bit analog-digital board DigiData 1440A (Molecular Devices, USA) under control of pClamp 10 software (Molecular Devices, USA) and stored for offline analysis. Action potentials and K^+ currents were

measured using modified Tyrode's solution (same as for contractility measurements) as superfusate and K^+ pipette solution containing in mmol/l: 30 KCl, 110 K-aspartate, 5 MgATP, 5 EGTA, 10 HEPES. Ca^{2+} current was measured with nominally K^+-free modified Tyrode's solution as superfusate and Cs^+ pipette solution containing in mmol/l: 25 CsCl, 5 NaCl, 110 CsOH, 110 aspartic acid, 5 MgATP, 5 EGTA, 10 HEPES. Small stabilizing hyperpolarizing current (–50...–75 pA) was constantly injected to ensure consistent and stable recording of action potentials. Late Na^+ current was measured with nominally K^+-free modified Tyrode's solution with 3 µmol/l nisoldipine (Sigma Aldrich, Canada) as superfusate and Cs^+ pipette solution.

K^+ currents were measured in myocytes superfused with modified Tyrode's solution and dialyzed with K^+ pipette solution. Total K^+ current was elicited in response to 500-ms depolarizations from –85 to +20 mV and reported as time-dependent ($I_{K,TD}$; peak – steady state) and steady-state ($I_{K,ss}$, the amplitude at the end of 500-ms depolarization). I_{K1} was elicited by 100-ms hyperpolarizations from –85 to –120 mV and reported as amplitude at 100-ms hyperpolarization. L-type Ca^{2+} current ($I_{Ca,L}$) was measured in myocytes superfused with nominally K^+-free modified Tyrode's solution and dialyzed with Cs^+ pipette solution. The current was elicited in response to step depolarization from –40 mV to 0 mV. Nisoldipine (3 µmol/l; Sigma Aldrich, USA) was used to record background current and isolate $I_{Ca,L}$. Late Na^+ current (I_{Na-L}) was measured in myocytes superfused with nominally K^+-/Ca^{2+}-free modified Tyrode's solution containing 1 µmol/l nisoldipine and dialyzed with Cs^+ pipette solution. The current was elicited by depolarizations from –120 (pre-pulse) to –40 mV. Tetrodotoxin in citrate buffer (5 µmol/l TTX, Abcam, USA) was used to record background and isolate I_{Na-L}. In general, currents were measured at 6-8 min dialysis time (baseline), then vehicle or drug was

applied for 6-8 min, followed by a specific blocker (*e.g.*, nisoldipine or TTX) if required to determine background current.

2.6. Ex-vivo epicardial optical mapping.

Simultaneous voltage and Ca^{2+} mapping were performed as described [30]. Hearts were cannulated and perfused using a Langendorff column with modified Krebs-Henseleit solution [1.2 or 3.6 mmol/l Ca^{2+}, 1 g/l albumin, 10 µmol/l (–)-blebbistatin under 70 mm Hg pressure (resulting in the flow rate of 1.5-2 ml/min) at 36-37 °C. After initial perfusion for 5-10 min, hearts were loaded with Ca^{2+}-sensitive dye Rhod-2AM (ThermoFisher Scientific, Canada) (80 µl per heart of 1 g/l solution) for 15 min followed by loading with voltage-sensitive dye RH237 (ThermoFisher Scientific, Canada) (60 µl per heart of 1 g/l solution) for 6 min. MiCAM Ultima (Brainvision Inc., Japan) was used to record and process optical signals from the hearts. Images were recorded at a frame rate of 1 kHz. Hearts were paced at 6 Hz (applied to the right atria). For arrhythmia induction, hearts were paced at 12 Hz for 1.5 s (applied to the left ventricle) and then allowed to excite autonomously. Baseline measurements were taken 5 min after loading the dyes. Drug or placebo was applied, followed by another measurement 7 min later. Action potential duration (APD) were reported as averages for the heart.

2.7. Electrocardiographic (ECG) recording and administration of BYL.

Mice were placed under isoflurane anesthesia (1.5-2%) on a heated pad (body temperature maintained at 37 °C, measured by the rectal probe). ECG leads were placed in

Lead I configuration. Signal was digitized using acquisition interface ACQ-7700 (Data Science International, USA) with P3 Plus software (ver. 5.0, Data Science International, USA). ECGs were recorded before administration of BYL or vehicle (base recording), followed by daily gavaging of the vehicle (corn oil) or BYL (30 mg/kg; dissolved in corn oil (3.75 g/l) for 4 days. Another ECG was taken 2 h after the last dose of vehicle or BYL, and change expressed as % control change from the base (the first measurement).

2.8. Immunoblot analysis.

For Western blots, cardiomyocytes were collected from plates and lysed using a CelLytic M Cell Lysis Reagent (Sigma Aldrich, Canada) with cOmplete and PhosSTOP inhibitors (Roche, Canada). Upon transfer to Immobilon PVDF membranes (EMD Millipore, Canada), antibodies used were from Cell Signaling (Product ID: 9272, 9271, 9275 and 7074). PVDF membranes were stained for total protein as a loading control using MemCode (Thermo Fisher Scientific).

2.9. Drugs.

The following drugs were used: BYL719 (BYL; ChemieTek, USA) as 10 µmol/l stock in DMSO, KB-R7943 mesylate (KB-R; Tocris Bioscience, USA) as 100 mmol/l stock in DMSO, Nisoldipine (Sigma Aldrich, USA) as 10 mmol/l stock in DMSO, ranolazine (Ran; Tocris Bioscience, USA) as 100 mmol/l stock in double-distilled water (ddH_2O), and tetrodotoxin in citrate buffer (TTX, Abcam, USA) as 10 mmol/l stock in ddH_2O. All stocks were stored at –20 °C.

2.10. Data transformation and statistics.

For statistical comparison, unless otherwise indicated, most measurements were expressed as absolute change from the baseline (Δ). Changes from baseline for vehicle group (Vehicle – $base_{vehicle}$) were compared with changes from baseline in the BYL (BYL – $base_{BYL}$) to account for non-specific changes with time. All vehicle measurements were vehicle time control, *i.e.*, the vehicle was applied at similar time points as drug applications. Comparisons between vehicle and drug applications were made using a non-paired Student's t-test or one-way ANOVA with Tukey post-hoc test as appropriate. Independent-sample Kruskal-Wallis test was used for non-parametric comparisons. Statistical analysis was performed using SPSS 25 software. Values are reported as mean ±SEM. Values of $p < 0.05$ are considered significant. Absolute values for baseline and measurement are provided in the supplemental figures as time series plots.

3. Results

3.1. Pharmacological inhibition of PI3Kα increases contractility of isolated cardiomyocytes.

Single-myocyte contractility was recorded at baseline and in the presence of increasing concentrations of BYL719 (vehicle, 10, 100, or 1000 nmol/l BYL). The resulting average traces showed a BYL dose-dependent increase in the amplitude of contraction (Figure 1A). Fractional shortening (FS), the rate of contraction (C, or –dL/dt max), and rate of relaxation (R, +dL/dt max) increased as BYL concentration increased, whereas the ratio of rates of relaxation to contraction (R/C) remained unchanged (Figure 1B). All measurements were expressed as a

percent change from their baseline (taken before application of either vehicle or BYL). BYL significantly increased fractional shortening (FS), the rate of contraction (C), and rate of relaxation (R) at both 100 nmol/l and 1000 nmol/l (Figure 1C). Increases in rates of contraction (C) and relaxation (R) were proportional as evident from lack of change in R/C (Figure 1B) and ΔR/C (Figure 1C).

To investigate the mechanism of BYL action, we selected the second highest concentration of BYL (100 nmol/l) that resulted in increased contractility (ΔFS and Δ–dL/dt) in isolated cardiomyocytes. BYL did not increase the contractility of PI3Kα-deficient myocytes (myocytes isolated from p110$\alpha^{flx/flx}$-αMHC-Cre mice, p110$\alpha^{f/f}$-Cre) (Figure 2A and Figure S1A), indicating that the BYL effect is PI3Kα specific. There is also a possibility that BYL cannot increase contractility in PI3Kα-deficient myocytes because the contractility is already saturated. We applied 1 µmol/l isoproterenol and found that PI3Kα-deficient myocytes has an increase in FS in response to isoproterenol (Figure S1B). Since diminished PI3Kα activity was linked to activation of $I_{Na\text{-}L}$ [15, 16, 26], we investigated the possible involvement of the late Na^+ current ($I_{Na\text{-}L}$) and Na^+-Ca^{2+} exchanger (NCX) by using $I_{Na\text{-}L}$ blocker, ranolazine (10 µM RAN; which predominantly blocks the late phase of the Na^+ current, but not the peak current) [31], and a reverse-mode NCX blocker, KB-R7943 (3 µM KB-R) [32] in WT cardiomyocytes. Both ranolazine and KB-R abolished the effect of BYL on contractility (Figure 2B,C and Figure S1C,D) suggesting the involvement of $I_{Na\text{-}L}$ as a source of Na^+ entry and NCX as a source of Ca^{2+} entry *via* reverse mode, promoting myocyte contractility.

3.2. Pharmacological inhibition of PI3Kα increases Ca^{2+} release in isolated cardiomyocytes.

Application of BYL increased the amplitude of Ca^{2+} transients (A_{Ca}) and decreased the time constant of clearing intracellular Ca^{2+} (τ_{Ca}) in WT myocytes (Figure 3A and Figure S2A), whereas PI3Kα-deficient myocytes (αCre) did not respond to BYL (Figure 3B and Figure S2B). In the presence of $I_{Na\text{-}L}$ blocker ranolazine, BYL failed to increase Ca^{2+} release (Figure 3C and Figure S2C), suggesting that the BYL effect on contractility is mediated *via* enhancement of sarcoplasmic reticulum (SR) Ca^{2+} release and $I_{Na\text{-}L}$.

3.3. Pharmacological inhibition of PI3Kα prolongs action potential in isolated cardiomyocytes.

In response to BYL, WT myocytes had prolonged action potential duration (APD) at repolarization levels 20%, 50%, and 90% (APD_{20}, APD_{50}, and APD_{90}). Repolarization phase was prolonged by 10-15% in the presence of BYL in control (Figure 4A and Figure S3A), but not in PI3Kα-deficient myocytes (Figure 4B and Figure S3B). In the presence of ranolazine, BYL failed to prolong action potentials at APD_{20} and APD_{90}, but some prolongation at APD_{50} remained (Figure 4C and Figure S3C). APD prolongation due to BYL can contribute to an increase in Ca^{2+} release due to additional Ca^{2+} influx *via* reverse mode of NCX with some contribution from L-type Ca^{2+} channels.

3.4. Identification of ionic currents regulated by PI3Kα in isolated cardiomyocytes.

Voltage clamp was used to determine changes in K^+-, Ca^{2+}-, and Na^+-currents underlying the prolongation of the action potential by BYL. Total K^+ current (I_{TO}, I_{slow}, and I_{ss}) was not

affected by BYL (Figure S4). L-type Ca^{2+} current ($I_{Ca,L}$) was inhibited by BYL in control myocytes (CTR; pooled p110$\alpha^{f/f}$ littermates and WT), but was unaffected in PI3Kα-deficient myocytes (p110$\alpha^{f/f}$-Cre) (Figure 5A and Figure S5A,B). The effects of BYL on contractility, Ca^{2+} transients, and action potentials suggest that PI3Kα activity is responsible for the suppression of I_{Na-L}. To test this, we compared the effects of PI3Kα activation with 0.2% FBS and 50 U/L insulin (FBS) by itself and in the presence of BYL (BYL+FBS) on I_{Na-L}. In the CTR group, activation of PI3Kα reduced late Na^+ current (I_{Na-L}), but not when PI3Kα was inhibited by BYL (Figure 5B and Figure S5C). To confirm that FBS mixture can activate PI3Kα and that 100 nmol/l BYL is sufficient to block this activation, we treated cultured myocytes with the vehicle, FBS mixture, or FBS mixture with BYL for 15 min. Immunoblotting of proteins from collected myocytes showed that FBS markedly upregulated Akt phosphorylation at both Thr308 and Ser473 and this phosphorylation was abrogated by BYL (Figure 5C and Figure S5D). Consistent with the notion that PI3Kα inhibits I_{Na-L}, PI3Kα-deficient myocytes (p110$\alpha^{f/f}$-Cre) had a considerably higher density of I_{Na-L} than that in CTR myocytes (Figure 5D,E). The current in the PI3Kα-deficient myocytes was insensitive to BYL (Figure 5D,E). Moreover, application of intracellular PIP3 ($PIP3_i$) in PI3Kα-deficient myocytes (p110$\alpha^{f/f}$-Cre) resulted in a substantial reduction of I_{Na-L} (Figure 5D,E). The current in PI3Kα-deficient myocytes was also sensitive to ranolazine (RAN), I_{Na-L} blocker (Figure 5D,E). Our data demonstrate that activation of PI3Kα suppresses late Na^+ current (I_{Na-L}), whereas the absence of PI3Kα is associated with increased I_{Na-L} density. PIP3, produced by PI3Kα, is the most probable mediator of PI3Kα-mediated I_{Na-L} suppression.

3.5. Pharmacological inhibition of PI3Kα in ex vivo hearts prolongs action potential, enhances Ca^{2+} release, and triggers arrhythmias.

Changes in voltage-sensitive fluorescence (action potentials, AP) and changes in Ca^{2+}-sensitive fluorescence (Ca^{2+} release) were optically recorded from *ex vivo* hearts. Application of BYL resulted in a small prolongation of the action potential (Figure 6A), similar to results obtained in isolated myocytes (Figure 4A), and a modest increase in the amplitude of Ca^{2+} release (Figure 6B), analogous to the changes in Ca^{2+} release at the cellular level (Figure 3A). Action potentials were affected measurably only at APD_{50}, (Figure 6C) whereas APD_{20} and APD_{90} remained unaffected (Figure S6). The amplitude of Ca^{2+} transient (A_{Ca}) increased by about 15% in the presence of 1.2 mM extracellular Ca^{2+} (Figure 6C; Figure S7 shows voltage- (V) and Ca^{2+}-fluorescent images of the representative heart). The ability of BYL to enhance Ca^{2+} release raises the question of whether the effect of BYL is additive or can be occluded by β-adrenergic stimulation. To explore this possibility, vehicle or BYL was applied in the presence of 200 nmol/l isoproterenol (Iso). BYL elicited an additional increase in Ca^{2+} release in the presence of Iso (Figure 6D,E), and 10 μmol/l ranolazine (RAN) prevented BYL-mediated increase in Ca^{2+} release in the presence of Iso (Figure 6D,E). Since excessive Ca^{2+} load of sarcoplasmic reticulum is potentially arrhythmogenic, [33, 34] we used arrhythmogenic protocol [isoproterenol (200 nmol/l) in combination with high Ca^{2+} (3.6 mM) and burst pacing (1.5 s at 12 Hz)] to provoke arrhythmic events [35]. In response to arrhythmogenic protocol, most littermate controls ($p110\alpha^{f/f}$) exhibited no arrhythmic events (1 out of 6 hearts tested had delayed afterdepolarizations, DAD; Figure 6F), and many PI3Kα-deficient hearts ($p110\alpha^{f/f}$-Cre) showed delayed afterdepolarization (4 out of 7; Figure 6F; Supplement Video DAD) with one heart

developing sustained ventricular fibrillation (Figure 6G; Supplement Video VFib). The DAD burden calculated as a sum of DAD events during 2-s post burst at 5, 7, and 9 min of exposure to isoproterenol and high Ca^{2+} was significantly higher in PI3Kα-deficient hearts in comparison to control hearts (Table S1).

3.6. Pharmacological inhibition of PI3Kα prolongs QT interval.

Control mice (CTR) were administered placebo or BYL for 4 days. Representative Lead I electrocardiograms (ECGs) for placebo and BYL are shown in Figure 7A, with absolute values of intervals RR, QRS, PR, and QT plotted in Figure 7B. Changes from the baseline in all intervals except QT were not significant (Figure 7C). QT interval exhibited 20% prolongation (not corrected) in response to BYL treatment, and QT corrected intervals (Bazett's correction, QT_{cB}, and Fridericia's correction, QT_{cF}) exhibited about 15% prolongation. The PI3Kα-deficient mice (p110$\alpha^{f/f}$-Cre) had longer QT interval than control mice (Figure 7B, D), and application of BYL failed to prolong QT, suggesting that BYL action is PI3Kα-dependent (Figure 7D,E).

4. Discussion

Development of new cancer therapies raises questions of possible adverse side effects, including heart-related side effects. This is especially the case for the PI3K pathway, which is very important not only for tumorigenesis and cancer progression but also plays a central role in the control of hypertrophy, contractility, and metabolism in the heart. Cancer therapeutics targeting PI3Kα specifically (taselisib, GDC0032 [6]; alpelisib, BYL719 [7, 8]; TAK117, MLN1117

[9]) along with other PI3Ks (pan-PI3K inhibitors; e.g., BKM120 [10]), or inadvertently (ibrutinib [12]) are in clinical trials.

Low PI3Kα activity is associated with arrhythmias. So far, QT interval prolongation has been reported for alpelisib (BYL719) [8] and copanlisib [5]. In the case of BYL719, hyperglycemia was common in all trials with PI3Kα inhibitors [6-9], which is consistent with systemic pharmacological inhibition of PI3Kα in mice [29]. Also, off-target inhibition of PI3Kα by ibrutinib is linked to increases in cardiac disorders (2-fold) and atrial fibrillation (3-fold) in comparison to the anti-CD20 monoclonal antibody ofatumumab [12], as well as instances of sudden death and ventricular arrhythmias in patients with no prior cardiac history [13, 14]. In mice, high doses of ibrutinib increase the susceptibility to induced atrial and ventricular arrhythmias, and this susceptibility was normalized on withdrawal of the drug [36]. Corroborating this point further, reduced activation of the PI3Kα pathway due to diabetes mellitus is also associated with prolongation of QTc interval [15, 16, 37, 38]. Various animal models of diabetes mellitus across many species exhibited prolongation of the action potential and QTc interval [37, 38], which is consistent with the idea that reduced sensitivity to insulin leads to diminished PI3Kα activity and prolongation of action potential [15, 16].

Pharmacokinetics of BYL. In our study, we mainly used 100 nmol/l BYL for *in vitro* and *ex vivo* experiments. This concentration is considerably less than plasma concentration achieved in the pre-clinical models and patients. In mice, 2-8 h after BYL treatment with prospective dosages of 25 mg/kg and 50 mg/kg, plasma concentrations achieved ~10-15 µmol/l and ~15-25 µmol/l, respectively, whereas the peak plasma concentration (1 h after treatment) reached 25 and 40 µmol/l for dosages of 25 mg/kg and 50 mg/kg, respectively [39]. In patients, BYL (300

mg daily) resulted in AUC_{tau} ~25,000 h ng/ml with T_{max} = 4 h, [8] which will be equivalent to average plasma concentration of ~14 μmol/l. A more detailed study on pharmacokinetics and pharmacodynamics of BYL in patients (daily dosage of 270-400 mg) reported median plasma concentrations 2,000-5,000 ng/ml (2-8h after treatment), which is equivalent to 4.5-11.3 μmol/l [40].

PI3Kα, excitation-contraction coupling, and arrhythmias. We showed that activation of PI3Kα leads to inhibition of I_{Na-L}. Conversely, inhibition of PI3Kα is known to activate (disinhibit) I_{Na-L} [19, 25, 26] most likely due to the production of PIP3 [25, 26]. Consistent with that framework we observed higher current densities of I_{Na-L} in PI3Kα-deficient myocytes. Active I_{Na-L} will produce an additional persistent depolarizing Na^+ influx (I_{Na-L}; see (1) in Figure 8A), which will increase cytosolic Ca^{2+} either *via* reverse mode of Na^+-Ca^{2+} exchanger or by reduction of Ca^{2+} extrusion via forward mode (2). Prevention of BYL effect by KB-R (a specific inhibitor of the reverse mode) suggests the involvement of reverse mode in the buildup of intracellular Ca^{2+}. Increased cytosolic Ca^{2+} will promote an increased Ca^{2+} load of the SR due to SERCa2 activity (3), which, in turn, will lead to enhanced Ca^{2+} release (4) and enhanced contractility (5) (Figure 8A). The increase in Ca^{2+} load was corroborated by increases in caffeine-induced Ca^{2+} release, Ca^{2+} transients (in myocytes and *ex vivo* hearts), and myocyte contractility. Surprisingly, PI3Kα-myocytes exhibited neither increased Ca^{2+} release nor contractility in comparison to normal myocytes suggesting that cardiac excitation-contraction coupling may adapt for the lack of PI3Kα signaling with time and/or during normal development. We were able to block the increases in Ca^{2+} release and contractility at step (1) by ranolazine (I_{Na-L} blocker) and step (2) by KB-R (reverse-mode NCX blocker). However, in our opinion, these seemingly beneficial

increases in contractility and Ca^{2+} release are the signs of potentially dangerous arrhythmias since the increases are achieved due to an increase in $I_{Na\text{-}L}$ and associated with increased Ca^{2+} load of the SR that can lead to prolongation of action potential, abnormal automaticity, early and delayed afterdepolarization, and increased dispersion of repolarization [41, 42]. Disinhibition of $I_{Na\text{-}L}$ due to suppression of PI3Kα activity (see (LQT) in Figure 8B) will produce additional depolarizing current that will prolong action potential producing a situation analogous to gain-of-function mutations in *SCN5A* that have been linked to arrhythmias (including long QT, LQT, and sudden cardiac death) and heart failure (dilated cardiomyopathy) [21-23, 43]. We observed prolongation of AP (in myocytes and *ex vivo* hearts) and QTc (in mice treated with BYL) suggesting that PI3Kα inhibitors may produce drug-induced LQT. Besides direct prolongation of the action potential, the additional influx of Na^+ *via* $I_{Na\text{-}L}$ will increase Ca^{2+} load of the SR (Figure 8B). That increase occurs independently of β-adrenergic stimulation and thus will add additional Ca^{2+} load creating a risky situation analogous to catecholaminergic polymorphic ventricular tachycardia (CPVT) [34, 44], which is characterized by excessive Ca^{2+} load from β-adrenergic stimulation (see (6) in Figure 8B). We observed BYL-induced increase in instances of delayed afterdepolarization in hearts under β-adrenergic stimulation suggesting that an excessive Ca^{2+} load may lead to spontaneous Ca^{2+} release (7) that will generate depolarizing current (I_{NCX}) *via* forward mode of NCX (8) producing DAD and possibly triggered activity (Figure 8B).

Arrhythmias as clinical implications of reduced PI3Kα activity. Arrhythmias generated by activation of $I_{Na\text{-}L}$ and additional Ca^{2+} influx *via* NCX that accompanies activation of $I_{Na\text{-}L}$ have been linked to the development of heart failure in murine pressure overload model [20]

possibly due to hypertrophic calcineurin-NFAT signaling [45]. In the case of overt heart failure, when β-adrenergic stimulation tries to maintain cardiac output [46], additional Ca^{2+} influx *via* NCX due to enhanced I_{Na-L} would aggravate the effects of β-adrenergic stimulation leading to the accelerated onset of heart failure. Moreover, pro-arrhythmic effects of I_{Na-L} disinhibition due to PI3Kα inhibition will be amplified because failing myocardium has high levels of Na^+-Ca^{2+} exchanger in humans [47] and rodent models [48]. The link between PI3Kα activity and heart failure is especially important for older cancer patients who are at considerable risk of comorbidities such as heart failure [49]. Another risk factor associated with inhibition of PI3Kα activity is polymorphisms in genes that are involved in all steps of generation of Ca^{2+} overload (Figure 8). First, genes that are responsible for Na^+ influx *via* I_{Na-L} (*SCN5A* and *SCN10A*). Polymorphisms in these genes have already been linked to heart failure (dilated cardiomyopathy) and arrhythmias (including sudden cardiac death) [21-23, 43]. LQT related polymorphisms and mutations in *SCN5A* or *SCN10A* may be aggravated by additional QTc prolongation due to disinhibition of I_{Na-L} that is carried *via SCN5A* and/or *SCN10A*. Second, polymorphisms and mutations related to CPVT. These mutations and polymorphisms will exacerbate sensitivity to Ca^{2+} overload [44] that may develop due to PI3Kα inhibition. A breadth of possibilities of polymorphisms and/or mutations involved in the development of cardiotoxicity may require the development of a carefully selected panel of genetic markers to screen cancer patients for possible adverse reactions to PI3Kα inhibition. A potential strategy for prevention of PI3Kα-related cardiotoxicity could be the use of a late Na^+ current blocker (e.g., ranolazine) [31] that, as shown here, was able to prevent AP prolongation, potentiation of Ca^{2+} release, and enhanced β-adrenergic stimulation resulting from inhibition of PI3Kα. Our

findings suggest that a reverse-mode Na^+-Ca^{2+} exchanger blocker can also be used to achieve similar results. Ranolazine will be a particularly fitting choice of adjuvant therapy because it has been shown to improve heart function in heart failure (not related to drug-induced cardiotoxicity) [50-52] as well as in the settings of anthracycline cardiotoxicity [53].

In conclusion, inhibition of PI3Kα is inherently pro-arrhythmic with a potential for drug-induced LQT. Although inhibition of PI3Kα can be tolerated by healthy hearts under quiescent conditions, it may present a significant risk in the cases of (i) excessive activation of β-adrenergic stimulation, (ii) heart failure (high levels of NCX), and/or (iii) in the presence of polymorphisms or mutations that prolong QTc (LQT syndromes), exacerbate Ca^{2+} overload (CPVT), or associated with risk of life-threatening arrhythmias (sudden cardiac death). Our findings suggest that administration of PI3Kα inhibitors may require monitoring of cardiac electrical activity for possible adverse electrophysiological side effects. Inhibition of late Na^+ current and/or reverse-mode Na^+-Ca^{2+} exchanger may be worthy of further investigation as a possible adjuvant therapy.

Limitations

BYL is a specific inhibitor of PI3Kα [39]. However, specificity in this context means that the inhibitor distinguishes between different isoforms of PI3K. PI3Kα is inhibited with IC_{50} ~ 5 nmol/l, which is ~50-fold lower than the closest IC_{50} for PI3Kγ [39]. Authors are not aware of any off-target activity of BYL719. Similarly, KB-R is a specific inhibitor of the reverse mode of NCX, but again specificity in this context means that the reverse mode is targeted over the

forward mode. KB-R is known to inhibit various membrane channels at concentrations that are necessary to inhibit the reverse mode [54-56]. Ranolazine is capable of inhibiting other isoforms of Na^+ channels besides $Na_V1.5$, delayed rectifier K^+ channels, and $I_{Ca,L}$ at much higher concentrations (IC50 ~ 300 μmol/l) [57, 58]. Ranolazine has been shown to upregulate RISK pathway, improve mitochondrial function, decrease reactive oxygen species production, and reduce apoptosis [59, 60]. Most of these off-target actions of ranolazine could not contribute to the ranolazine action in isolated myocytes or whole-hearts except for the activation of the RISK pathway, whose activation will lead to activation of ATP-dependent K^+ channels in the cellular and mitochondrial membrane. Activation of K^+ (ATP) channels may have contributed to the shortening of action potential however since the effect of BYL was defined as change from the baseline, such measure is relatively insensitive to the changes of the baseline value itself.

Sources of Funding

We acknowledge funding support from the Canadian Institutes of Health Research (CIHR). Dr. Oudit's research is supported by a Tier 2 Canada Research Chair in Heart Failure through the Government of Canada (Ottawa, Ontario).

Disclosures: NONE

REFERENCES

[1] Crackower MA, Oudit GY, Kozieradzki I, Sarao R, Sun H, Sasaki T, et al. Regulation of myocardial contractility and cell size by distinct PI3K-PTEN signaling pathways. Cell. 2002;110(6):737-49.

[2] McLean BA, Zhabyeyev P, Pituskin E, Paterson I, Haykowsky MJ, Oudit GY. PI3K inhibitors as novel cancer therapies: implications for cardiovascular medicine. Journal of cardiac failure. 2013;19(4):268-82.

[3] Vanhaesebroeck B, Whitehead MA, Pineiro R. Molecules in medicine mini-review: isoforms of PI3K in biology and disease. J Mol Med (Berl). 2016;94(1):5-11.

[4] Mayer IA, Arteaga CL. The PI3K/AKT Pathway as a Target for Cancer Treatment. Annual review of medicine. 2016;67:11-28.

[5] Curigliano G, Shah RR. Safety and Tolerability of Phosphatidylinositol-3-Kinase (PI3K) Inhibitors in Oncology. Drug Saf. 2019;42(2):247-62.

[6] Juric D, Krop I, Ramanathan RK, Wilson TR, Ware JA, Sanabria Bohorquez SM, et al. Phase I Dose-Escalation Study of Taselisib, an Oral PI3K Inhibitor, in Patients with Advanced Solid Tumors. Cancer discovery. 2017;7(7):704-15.

[7] Mayer IA, Abramson VG, Formisano L, Balko JM, Estrada MV, Sanders ME, et al. A Phase Ib Study of Alpelisib (BYL719), a PI3Kalpha-Specific Inhibitor, with Letrozole in ER+/HER2- Metastatic Breast Cancer. Clinical cancer research : an official journal of the American Association for Cancer Research. 2017;23(1):26-34.

[8] van Geel R, Tabernero J, Elez E, Bendell JC, Spreafico A, Schuler M, et al. A Phase Ib Dose-Escalation Study of Encorafenib and Cetuximab with or without Alpelisib in Metastatic BRAF-Mutant Colorectal Cancer. Cancer discovery. 2017;7(6):610-9.

[9] Juric D, de Bono JS, LoRusso PM, Nemunaitis J, Heath EI, Kwak EL, et al. A First-in-Human, Phase I, Dose-Escalation Study of TAK-117, a Selective PI3Kalpha Isoform Inhibitor, in Patients with Advanced

Solid Malignancies. Clinical cancer research : an official journal of the American Association for Cancer Research. 2017.

[10] Rodon J, Brana I, Siu LL, De Jonge MJ, Homji N, Mills D, et al. Phase I dose-escalation and -expansion study of buparlisib (BKM120), an oral pan-Class I PI3K inhibitor, in patients with advanced solid tumors. Invest New Drugs. 2014;32(4):670-81.

[11] McMullen JR, Boey EJ, Ooi JY, Seymour JF, Keating MJ, Tam CS. Ibrutinib increases the risk of atrial fibrillation, potentially through inhibition of cardiac PI3K-Akt signaling. Blood. 2014;124(25):3829-30.

[12] Byrd JC, Brown JR, O'Brien S, Barrientos JC, Kay NE, Reddy NM, et al. Ibrutinib versus ofatumumab in previously treated chronic lymphoid leukemia. The New England journal of medicine. 2014;371(3):213-23.

[13] Tomcsanyi J, Nenyei Z, Matrai Z, Bozsik B. Ibrutinib, an Approved Tyrosine Kinase Inhibitor as a Potential Cause of Recurrent Polymorphic Ventricular Tachycardia. JACC Clin Electrophysiol. 2016;2(7):847-9.

[14] Lampson BL, Yu L, Glynn RJ, Barrientos JC, Jacobsen ED, Banerji V, et al. Ventricular arrhythmias and sudden death in patients taking ibrutinib. Blood. 2017;129(18):2581-4.

[15] Lu Z, Jiang YP, Wu CY, Ballou LM, Liu S, Carpenter ES, et al. Increased persistent sodium current due to decreased PI3K signaling contributes to QT prolongation in the diabetic heart. Diabetes. 2013;62(12):4257-65.

[16] Ballou LM, Lin RZ, Cohen IS. Control of cardiac repolarization by phosphoinositide 3-kinase signaling to ion channels. Circulation research. 2015;116(1):127-37.

[17] Yang KC, Foeger NC, Marionneau C, Jay PY, McMullen JR, Nerbonne JM. Homeostatic regulation of electrical excitability in physiological cardiac hypertrophy. The Journal of physiology. 2010;588(Pt 24):5015-32.

[18] Yang KC, Jay PY, McMullen JR, Nerbonne JM. Enhanced cardiac PI3Kalpha signalling mitigates arrhythmogenic electrical remodelling in pathological hypertrophy and heart failure. Cardiovascular research. 2012;93(2):252-62.

[19] Yang T, Chun YW, Stroud DM, Mosley JD, Knollmann BC, Hong C, et al. Screening for acute IKr block is insufficient to detect torsades de pointes liability: role of late sodium current. Circulation. 2014;130(3):224-34.

[20] Toischer K, Hartmann N, Wagner S, Fischer TH, Herting J, Danner BC, et al. Role of late sodium current as a potential arrhythmogenic mechanism in the progression of pressure-induced heart disease. Journal of molecular and cellular cardiology. 2013;61:111-22.

[21] Walsh R, Thomson KL, Ware JS, Funke BH, Woodley J, McGuire KJ, et al. Reassessment of Mendelian gene pathogenicity using 7,855 cardiomyopathy cases and 60,706 reference samples. Genet Med. 2017;19(2):192-203.

[22] Kääb S, Schulze-Bahr E. Susceptibility genes and modifiers for cardiac arrhythmias. Cardiovascular research. 2005;67(3):397-413.

[23] Zhabyeyev P, Oudit GY. Mechanisms of Cardiac Arrhythmias: Molecular and Cellular Perspective. In: Caplan M, editor. Reference Module in Biomedical Sciences: Elsevier; 2017.

[24] Zhabyeyev P, McLean B, Vanhaesebroeck B, Oudit GY. Acute Pharmacological Inhibition of PI3K alpha by the Novel Cancer Drug, BYL-719, Has a Pro-arrhythmic Effect. Circulation. 2016;134:A15697.

[25] Lu Z, Wu CY, Jiang YP, Ballou LM, Clausen C, Cohen IS, et al. Suppression of phosphoinositide 3-kinase signaling and alteration of multiple ion currents in drug-induced long QT syndrome. Science translational medicine. 2012;4(131):131ra50.

[26] Yang T, Meoli DF, Moslehi J, Roden DM. Inhibition of the alpha-Subunit of Phosphoinositide 3-Kinase in Heart Increases Late Sodium Current and Is Arrhythmogenic. The Journal of pharmacology and experimental therapeutics. 2018;365(3):460-6.

[27] Antzelevitch C, Burashnikov A. Overview of Basic Mechanisms of Cardiac Arrhythmia. Card Electrophysiol Clin. 2011;3(1):23-45.

[28] Graupera M, Guillermet-Guibert J, Foukas LC, Phng LK, Cain RJ, Salpekar A, et al. Angiogenesis selectively requires the p110alpha isoform of PI3K to control endothelial cell migration. Nature. 2008;453(7195):662-6.

[29] McLean BA, Zhabyeyev P, Patel VB, Basu R, Parajuli N, DesAulniers J, et al. PI3Kalpha is essential for the recovery from Cre/tamoxifen cardiotoxicity and in myocardial insulin signalling but is not required for normal myocardial contractility in the adult heart. Cardiovascular research. 2015;105(3):292-303.

[30] Salama G, Hwang SM. Simultaneous optical mapping of intracellular free calcium and action potentials from Langendorff perfused hearts. Curr Protoc Cytom. 2009;Chapter 12:Unit 12 7.

[31] Fischer TH, Herting J, Mason FE, Hartmann N, Watanabe S, Nikolaev VO, et al. Late INa increases diastolic SR-Ca2+-leak in atrial myocardium by activating PKA and CaMKII. Cardiovascular research. 2015;107(1):184-96.

[32] Satoh H, Ginsburg KS, Qing K, Terada H, Hayashi H, Bers DM. KB-R7943 block of Ca^{2+} influx via Na^{+}/Ca^{2+} exchange does not alter twitches or glycoside inotropy but prevents Ca^{2+} overload in rat ventricular myocytes. Circulation. 2000;101(12):1441-6.

[33] Fink M, Noble PJ, Noble D. Ca(2)(+)-induced delayed afterdepolarizations are triggered by dyadic subspace Ca2(2)(+) affirming that increasing SERCA reduces aftercontractions. Am J Physiol Heart Circ Physiol. 2011;301(3):H921-35.

[34] Zhabyeyev P, Hiess F, Wang R, Liu Y, Wayne Chen SR, Oudit GY. S4153R is a gain-of-function mutation in the cardiac Ca^{2+} release channel ryanodine receptor associated with catecholaminergic polymorphic ventricular tachycardia and paroxysmal atrial fibrillation. Can J Cardiol. 2013;29(8):993-6.

[35] Willis BC, Pandit SV, Ponce-Balbuena D, Zarzoso M, Guerrero-Serna G, Limbu B, et al. Constitutive Intracellular Na^{+} Excess in Purkinje Cells Promotes Arrhythmogenesis at Lower Levels of Stress Than

Ventricular Myocytes From Mice With Catecholaminergic Polymorphic Ventricular Tachycardia. Circulation. 2016;133(24):2348-59.

[36] Tuomi JM, Xenocostas A, Jones DL. Increased Susceptibility for Atrial and Ventricular Cardiac Arrhythmias in Mice Treated With a Single High Dose of Ibrutinib. Can J Cardiol. 2018;34(3):337-41.

[37] Lengyel C, Virag L, Biro T, Jost N, Magyar J, Biliczki P, et al. Diabetes mellitus attenuates the repolarization reserve in mammalian heart. Cardiovascular research. 2007;73(3):512-20.

[38] Zhang Y, Xiao J, Lin H, Luo X, Wang H, Bai Y, et al. Ionic mechanisms underlying abnormal QT prolongation and the associated arrhythmias in diabetic rabbits: a role of rapid delayed rectifier K^+ current. Cellular physiology and biochemistry : international journal of experimental cellular physiology, biochemistry, and pharmacology. 2007;19(5-6):225-38.

[39] Fritsch C, Huang A, Chatenay-Rivauday C, Schnell C, Reddy A, Liu M, et al. Characterization of the novel and specific PI3Kalpha inhibitor NVP-BYL719 and development of the patient stratification strategy for clinical trials. Molecular cancer therapeutics. 2014;13(5):1117-29.

[40] De Buck SS, Jakab A, Boehm M, Bootle D, Juric D, Quadt C, et al. Population pharmacokinetics and pharmacodynamics of BYL719, a phosphoinositide 3-kinase antagonist, in adult patients with advanced solid malignancies. Br J Clin Pharmacol. 2014;78(3):543-55.

[41] Shryock JC, Song Y, Rajamani S, Antzelevitch C, Belardinelli L. The arrhythmogenic consequences of increasing late INa in the cardiomyocyte. Cardiovascular research. 2013;99(4):600-11.

[42] Antzelevitch C, Nesterenko V, Shryock JC, Rajamani S, Song Y, Belardinelli L. The role of late I Na in development of cardiac arrhythmias. Handbook of experimental pharmacology. 2014;221:137-68.

[43] Tayal U, Prasad S, Cook SA. Genetics and genomics of dilated cardiomyopathy and systolic heart failure. Genome Med. 2017;9(1):20.

[44] Priori SG, Chen SR. Inherited dysfunction of sarcoplasmic reticulum Ca2+ handling and arrhythmogenesis. Circulation research. 2011;108(7):871-83.

[45] Dewenter M, von der Lieth A, Katus HA, Backs J. Calcium Signaling and Transcriptional Regulation in Cardiomyocytes. Circulation research. 2017;121(8):1000-20.

[46] Najafi A, Sequeira V, Kuster DW, van der Velden J. beta-adrenergic receptor signalling and its functional consequences in the diseased heart. European journal of clinical investigation. 2016;46(4):362-74.

[47] Flesch M, Schwinger RH, Schiffer F, Frank K, Sudkamp M, Kuhn-Regnier F, et al. Evidence for functional relevance of an enhanced expression of the Na^{+}-Ca^{2+} exchanger in failing human myocardium. Circulation. 1996;94(5):992-1002.

[48] O'Rourke B, Kass DA, Tomaselli GF, Kaab S, Tunin R, Marban E. Mechanisms of altered excitation-contraction coupling in canine tachycardia-induced heart failure, I: experimental studies. Circulation research. 1999;84(5):562-70.

[49] Sarfati D, Koczwara B, Jackson C. The impact of comorbidity on cancer and its treatment. CA Cancer J Clin. 2016;66(4):337-50.

[50] Hale SL, Shryock JC, Belardinelli L, Sweeney M, Kloner RA. Late sodium current inhibition as a new cardioprotective approach. Journal of molecular and cellular cardiology. 2008;44(6):954-67.

[51] Sossalla S, Wagner S, Rasenack EC, Ruff H, Weber SL, Schondube FA, et al. Ranolazine improves diastolic dysfunction in isolated myocardium from failing human hearts--role of late sodium current and intracellular ion accumulation. Journal of molecular and cellular cardiology. 2008;45(1):32-43.

[52] Maier LS, Layug B, Karwatowska-Prokopczuk E, Belardinelli L, Lee S, Sander J, et al. RAnoLazIne for the treatment of diastolic heart failure in patients with preserved ejection fraction: the RALI-DHF proof-of-concept study. JACC Heart failure. 2013;1(2):115-22.

[53] Minotti G. Pharmacology at work for cardio-oncology: ranolazine to treat early cardiotoxicity induced by antitumor drugs. The Journal of pharmacology and experimental therapeutics. 2013;346(3):343-9.

[54] Birinyi P, Acsai K, Banyasz T, Toth A, Horvath B, Virag L, et al. Effects of SEA0400 and KB-R7943 on Na+/Ca2+ exchange current and L-type Ca2+ current in canine ventricular cardiomyocytes. Naunyn Schmiedebergs Arch Pharmacol. 2005;372(1):63-70.

[55] Abramochkin DV, Alekseeva EI, Vornanen M. Inhibition of the cardiac inward rectifier potassium currents by KB-R7943. Comp Biochem Physiol C Toxicol Pharmacol. 2013;158(3):181-6.

[56] Abramochkin DV, Vornanen M. Inhibition of the cardiac ATP-dependent potassium current by KB-R7943. Comp Biochem Physiol A Mol Integr Physiol. 2014;175:38-45.

[57] Schram G, Zhang L, Derakhchan K, Ehrlich JR, Belardinelli L, Nattel S. Ranolazine: ion-channel-blocking actions and in vivo electrophysiological effects. Br J Pharmacol. 2004;142(8):1300-8.

[58] Kahlig KM, Lepist I, Leung K, Rajamani S, George AL. Ranolazine selectively blocks persistent current evoked by epilepsy-associated Nanu1.1 mutations. Br J Pharmacol. 2010;161(6):1414-26.

[59] Efentakis P, Andreadou I, Bibli SI, Vasileiou S, Dagres N, Zoga A, et al. Ranolazine triggers pharmacological preconditioning and postconditioning in anesthetized rabbits through activation of RISK pathway. Eur J Pharmacol. 2016;789:431-8.

[60] Zou D, Geng N, Chen Y, Ren L, Liu X, Wan J, et al. Ranolazine improves oxidative stress and mitochondrial function in the atrium of acetylcholine-CaCl2 induced atrial fibrillation rats. Life Sci. 2016;156:7-14.

Figure Legends

Figure 1. PI3Kα inhibition with BYL increases contractility of isolated ventricular myocytes in a dose-dependent manner. **A**. Average time courses of change in sarcomere length before (base, black) and after (measurement, red) application of vehicle (0), 10, 100, or 1000 nmol/l (nM) BYL. **B**. Time series plots of absolute values for fractional shortening (FS), the rate of contraction (C, –dL/dt), the rate of relaxation (R, +dL/dt), and the ratio of R to C (R/C). Open symbols represent baseline and filled symbols are either vehicle (0) or BYL (10, 100, or 1000 nM); n = 12-14 myocytes per group (50 myocytes from 9 hearts) **C**. Absolute change from baseline Δ = measurement – baseline for the data plotted in B. * $p < 0.05$ compared with vehicle (ANOVA with Tukey post-hoc test). Fraction by the box graphs represents p close to 0.05 for comparison with the vehicle. Field stimulation at 1 Hz.

Figure 2. Loss of BYL effect on contractility of isolated ventricular myocytes in PI3Kα-deficient model and by pharmacological interventions. **A**. Lack of BYL effect on contractility in PI3Kα-deficient myocytes (p110$\alpha^{f/f}$-Cre); n = 9-10 myocytes per group (19 myocytes from 4 hearts). **B**. Lack of BYL effect on contractility in the presence of 10 µmol/l ranolazine (Ran); n = 8-12 myocytes per group (20 myocytes from 4 hearts). **C**. Lack of BYL effect on contractility in the presence of 3 µmol/l KB-R7943 (KB-R); n = 8-9 myocytes per group (17 myocytes from 4 hearts). In all panels (**A**-**C**), average time courses of change in fractional shortening (FS), the rate of contraction (C, –dL/dt), and rate of relaxation (R, +dL/dt) are plotted on the right. The time

course before (black) and after (red) application of vehicle (0) or 100 nmol/l BYL. CTR is wild-type (WT) and p110$\alpha^{f/f}$ littermates of p110$\alpha^{f/f}$-Cre mice. Field stimulation at 1 Hz.

Figure 3. Effect of BYL on Ca^{2+} transients in isolated ventricular myocytes and ablation of the effect in PI3Kα-deficient myocytes and by pharmacological inhibition. **A**. BYL enhances Ca^{2+} transients in control myocytes (CTR); n = 13-15 myocytes per group (28 myocytes from 6 hearts). **B**. Lack of BYL effect on Ca^{2+} transients in PI3Kα-deficient myocytes (p110$\alpha^{f/f}$-Cre); n = 7-8 myocytes per group (15 myocytes from 4 hearts). **C**. Lack of BYL effect on Ca^{2+} transients in CTR myocytes in the presence of 10 µmol/l ranolazine (10 µM Ran); n = 8-9 myocytes per group (17 myocytes from 4 hearts). **D**. BYL enhances caffeine-induced Ca^{2+} release, and ranolazine prevents the effect of BYL. Representative releases are plotted on the left, and absolute values of amplitudes of Ca^{2+} releases (max A_{Ca}) are plotted on the right; n = 8-9 (25 myocytes from 6 hearts). In **A**-**C**, myocytes were field stimulated at 1 Hz, and average time courses of Ca^{2+} transients are plotted on the left, and change from baseline (Δ) for Ca^{2+} transient amplitude (A_{Ca}), the time constant of the decay (τ_{Ca}), and diastolic Ca (Ca_D) are plotted on the right. The time course before (black) and after (red) application of vehicle (0) or 100 nmol/l BYL. CTR is wild-type (WT) and p110$\alpha^{f/f}$ littermates of p110$\alpha^{f/f}$-Cre mice. * $p < 0.05$ compared with vehicle; # $p < 0.05$ compared with BYL group.

Figure 4. Effect of BYL on action potential in isolated ventricular myocytes and ablation of the effect in the PI3Kα-deficient model and by pharmacological intervention. **A**. BYL prolongs action

potential in control (CTR) myocytes; n = 9-10 myocytes per group (19 myocytes from 4 hearts). **B**. Lack of BYL effect on action potential in PI3Kα-deficient myocytes (p110$\alpha^{f/f}$-Cre); n = 7-8 myocytes per group (15 myocytes from 4 hearts). **C**. Lack of BYL effect on action potential in CTR myocytes in the presence of 10 µmol/l ranolazine (10 µM Ran); n = 9-10 myocytes per group (19 myocytes from 4 hearts). In all panels (**A**-**C**), representative action potentials are plotted on the left, and change in action potential duration (ΔAPD) at repolarization levels 20%, 50%, and 90% are plotted on the right. The action potentials before (black) and after (red) application of vehicle or 100 nmol/l BYL. CTR is wild-type (WT) and p110$\alpha^{f/f}$ littermates of p110$\alpha^{f/f}$-Cre mice. * $p < 0.05$ compared with vehicle.

Figure 5. Effect of inhibition and activation of PI3Kα on ionic currents in isolated ventricular myocytes. **A**. Inhibition of L-type Ca^{2+} current ($I_{Ca,L}$) by 100 nmol/l BYL and lack of the effect of BYL in PI3Kα-deficient myocytes (p110$\alpha^{f/f}$-Cre). Representative records of $I_{Ca,L}$ for control myocytes (CTR) in response to depolarization from –40 to 0 mV [before (black) and after (red) application of vehicle or 100 nmol/l BYL] (left). Change in amplitude of the peak $I_{Ca,L}$ ($\Delta I_{Ca,L}$) (right); n = 7-11 per group (34 myocytes; 8 hearts). **B**. Inhibition of late Na^+ current ($I_{Na\text{-}L}$) by FBS and diminished inhibition by FBS + 100 nmol/l BYL (FBS + BYL); n = 6-7 myocytes per group (13 myocytes; 4 hearts). **C**. Activation of PI3Kα by FBS and inhibition of PI3Kα by FBS + 100 nmol/l BYL (+BYL) in cultured isolated CTR cardiomyocytes. Ctl is control (no FBS, no BYL); n = 4 blots from 2 hearts. **D**. Current densities of $I_{Na\text{-}L}$ in normal (CTR) and PI3Kα-deficient myocytes (p110$\alpha^{f/f}$-Cre) for vehicle (Veh), 100 nmol/l BYL (BYL), 1 µmol/l intracellular PIP3 ($PIP3_i$), and 10

µmol/l ranolazine (RAN); n = 5-11 myocytes per group (36 myocytes; 9 hearts). **E**. Representative traces of late Na^+ current (I_{Na-L}) for conditions listed in *D*; times listed are post-dialysis time. In **D** and **E**, late Na^+ current (I_{Na-L}) was invoked in response to 500-ms depolarization from –120 to –40 mV and was measured as TTX-sensitive current at the end of 500-ms depolarization. Representative records: current before intervention (black), after intervention (red), and background (blue, +5 µmol/l TTX). FBS, a mixture of 0.2% fetal bovine serum with 50 U/L insulin (FBS); CTR, WT and p110$\alpha^{f/f}$ littermates. * $p < 0.05$ compared with vehicle; # $p < 0.05$ compared with FBS.

Figure 6. BYL prolongs action potential, enhances Ca^{2+} release, and trigger arrhythmias in *ex vivo* hearts. **A**. Representative action potentials before (black) and after (red) application of 100 nmol/l BYL, paced at 6 Hz. **B**. Representative traces of Ca^{2+} release before (black) and after (red) application of 100 nmol/l BYL, paced at 6 Hz. **C**. Change in the action potential duration at 50% repolarization (APD_{50}) and in the amplitude of Ca^{2+} transient due to application of vehicle or BYL, paced at 6 Hz; n = 6-7. **D**. Representative traces of Ca^{2+} transients before (black) and after (red) application of vehicle, 100 nmol/l BYL (BYL), or 10 µmol/l RAN + 100 nmol/l BYL (RAN + BYL) in the presence of 200 nmol/l of isoproterenol; paced at 12 Hz. **E**. Change in the amplitude of Ca^{2+} transients in the presence of 200 nmol/l of isoproterenol in response to application of vehicle, 100 nmol/l BYL (BYL), or 10 µmol/l RAN + 100 nmol/l BYL (RAN + BYL); paced at 12 Hz, n = 8-9. **F**. Representative frame and traces for p110$\alpha^{f/f}$ littermate (p110$\alpha^{f/f}$) (left) and PI3Kα-deficient hearts (p110$\alpha^{f/f}$-Cre) (right) in the presence of 3.6 mmol/l Ca^{2+} + 200 nM isoproterenol (Iso) in response to burst pacing for 1.5 s at 12 Hz. Instances of delayed afterdepolarizations are

marked with arrows; calibration bar 5 %F and 400 ms. **G**. An instance of ventricular fibrillation in PI3Kα-deficient heart (p110$\alpha^{f/f}$-Cre) heart in response to application of 200 nmol/l isoproterenol (Iso) in the presence of 3.6 mmol/l Ca^{2+}; calibration bar 2 %F and 20 ms. * $p < 0.05$ compared with vehicle. # $p < 0.05$ compared with BYL.

Figure 7. BYL prolongs QT interval in a PI3Kα-dependent manner. **A**. Representative pairs of electrocardiographic (ECG) traces for WT and p110$\alpha^{f/f}$ littermate mice (CTR): before (base) and after administration of the vehicle (left) and before (base) and after administration of BYL (right). **B**. Interval duration for RR, PR, and QT intervals for CTR mice. **C**. Change in the duration of RR, QT, QT_{cB} (Bazett correction), and QT_{cF} (Fridericia correction) calculated from values in B. **D**. Interval duration for RR, PR, and QT intervals for PI3Kα-deficient mice (p110$\alpha^{f/f}$-Cre). **E**. Change in the duration of RR, QT, QT_{cB} (Bazett correction), and QT_{cF} (Fridericia correction) calculated from values in D. * $p < 0.05$ compared with vehicle, ‡ $p < 0.05$ for comparison between pooled baselines.

Figure 8. PI3Kα, Ca^{2+} cycling, contractility, and arrhythmias. **A**. Enhanced Ca^{2+} release and contractility due to PI3Kα inhibition. (1) PIP3 produced by PI3Kα suppresses activation of late Na^+ current ($I_{Na\text{-}L}$). Once PI3Kα is inhibited by BYL, lack of PIP3 activates (dis-inhibits) $I_{Na\text{-}L}$, and additional Na^+ flows into the cell during an action potential. (2) Additional Na^+ is exchanged for additional intracellular Ca^{2+} *via* reverse mode of Na^+-Ca^{2+} exchanger (NCX). (3) Additional Ca^{2+} is re-uptaken into sarcoplasmic reticulum (SR) *via* sarco-endoplasmic reticulum Ca^{2+}-ATPase

(SERCa2) increasing Ca^{2+} load of the SR. (4) Increased Ca^{2+} load leads to larger Ca^{2+} release *via* Ca^{2+} release channels (RYR2) and, in turn, (5) enhanced contractility. Ca^{2+} build up in the SR can be interrupted at step (1) by ranolazine ($I_{Na\text{-}L}$ blocker) or step (2) by KB-R (reverse-mode NCX blocker). **B**. Pro-arrhythmic effects of PI3Kα inhibition. (LQT) Inhibition of PI3Kα (*e.g.*, BYL) will activate (dis-inhibits) $I_{Na\text{-}L}$, a depolarizing current, that may directly prolong action potential. Pro-arrhythmic action due to (6) Ca^{2+} overload (β-adrenergic stimulation and PI3Kα inhibition) is initiated by (7) spontaneous Ca^{2+} release *via* RYR2. Excess of Ca^{2+} is exchanged for Na^{+} (8) generating net inward (depolarizing current) current *via* NCX (I_{NCX}; 3 Na^{+} – 1 Ca^{2+} = 1+ net transfer into the cell). The depolarizing I_{NCX} produces membrane depolarization (delayed afterdepolarization, DAD) that may result in triggered activity. LTCC, L-type Ca^{2+} channel.

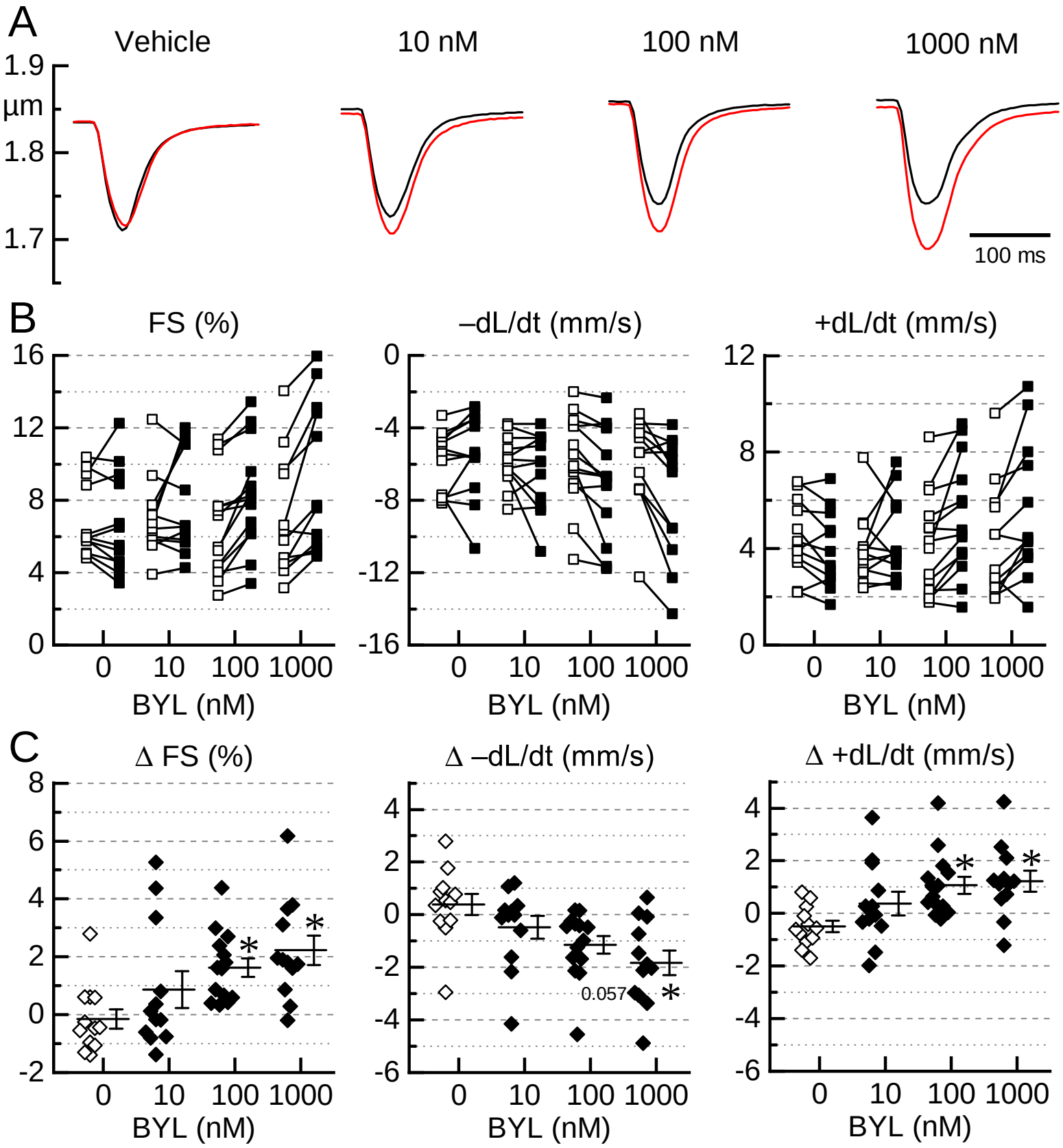

Figure 1. PI3Ka inhibition with BYL increases contractility of isolated ventricular myocytes in a dose-dependent manner. **A**. Average time courses of change in sarcomere length before (base, black) and after (measurement, red) application of vehicle (0), 10, 100, or 1000 nmol/l (nM) BYL. **B**. Time series plots of absolute values for fractional shortening (FS), rate of contraction (C, –dL/dt), rate of relaxation (R, +dL/dt), and ratio of R to C (R/C). Open symbols represent baseline and filled symbols are either vehicle (0) or BYL (10, 100, or 1000 nM); n = 12-14 myocytes per group (50 myocytes from 9 hearts) **C**. Absolute change from baseline Δ = measurement – baseline for the data plotted in B. * $p < 0.05$ compared with vehicle (ANOVA with Tukey post-hoc test). Fraction by the box graphs represents p close to 0.05 for comparison with vehicle. Field stimulation at 1 Hz.

Zhabyeyev P. et al. (2019)

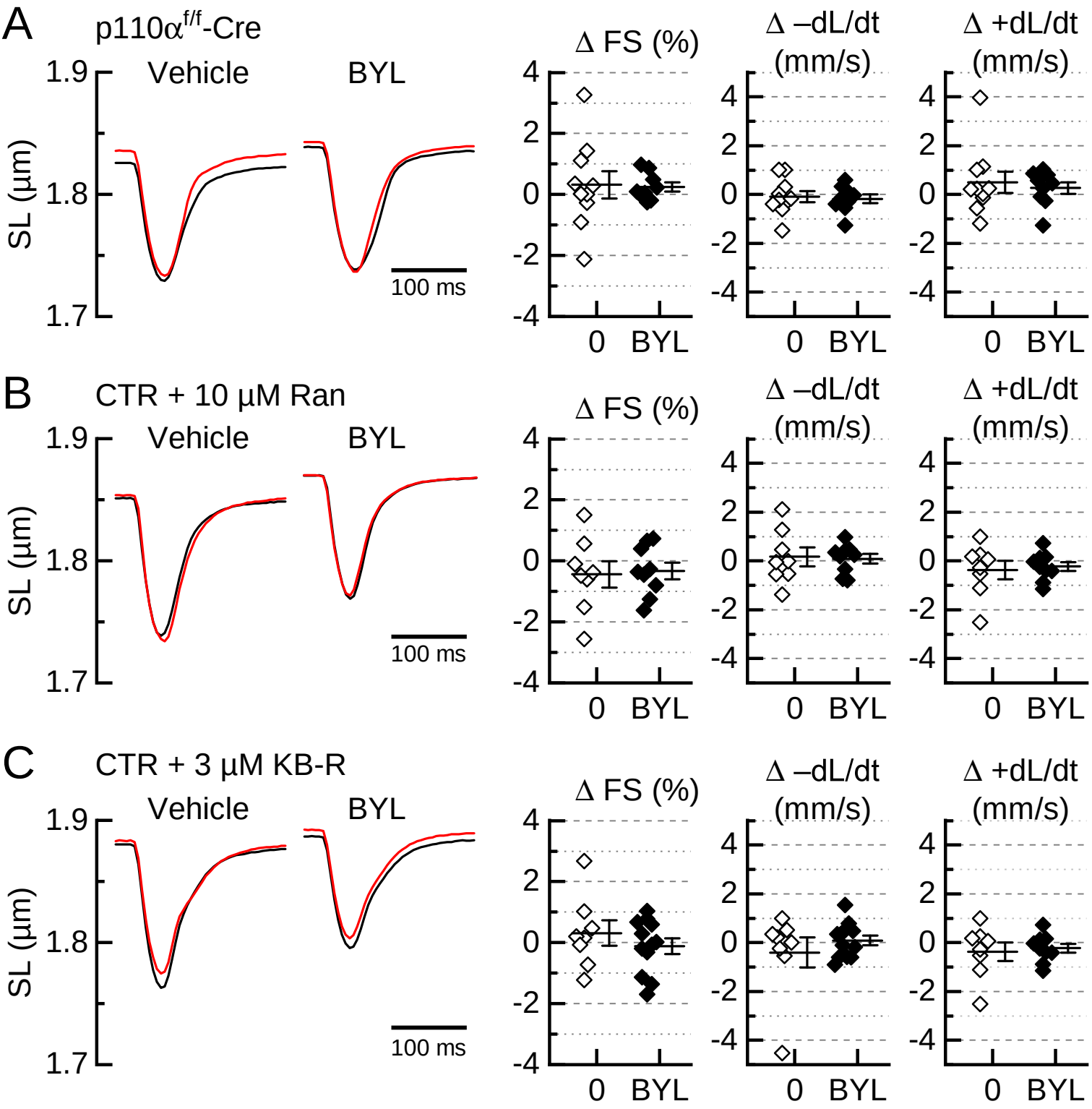

Figure 2. Loss of BYL effect on contractility of isolated ventricular myocytes in PI3Kα-deficient model and by pharmacological interventions. **A**. Lack of BYL effect on contractility in PI3Kα-deficient myocytes (p110α$^{f/f}$-Cre); n = 9-10 myocytes per group (19 myocytes from 4 hearts). **B**. Lack of BYL effect on contractility in the presence of 10 µmol/l ranolazine (Ran); n = 8-12 myocytes per group (20 myocytes from 4 hearts). **C**. Lack of BYL effect on contractility in the presence of 3 µmol/l KB-R7943 (KB-R); n = 8-9 myocytes per group (17 myocytes from 4 hearts). In all panels (**A**-**C**), average time courses of change in fractional shortening (FS), rate of contraction (C, –dL/dt), and rate of relaxation (R, +dL/dt) are plotted on the right. The time course before (black) and after (red) application of vehicle (0) or 100 nmol/l BYL. CTR is wild-type (WT) and p110α$^{f/f}$ littermates of p110α$^{f/f}$-Cre mice. Field stimulation at 1 Hz.

Zhabyeyev P. et al. (2019)

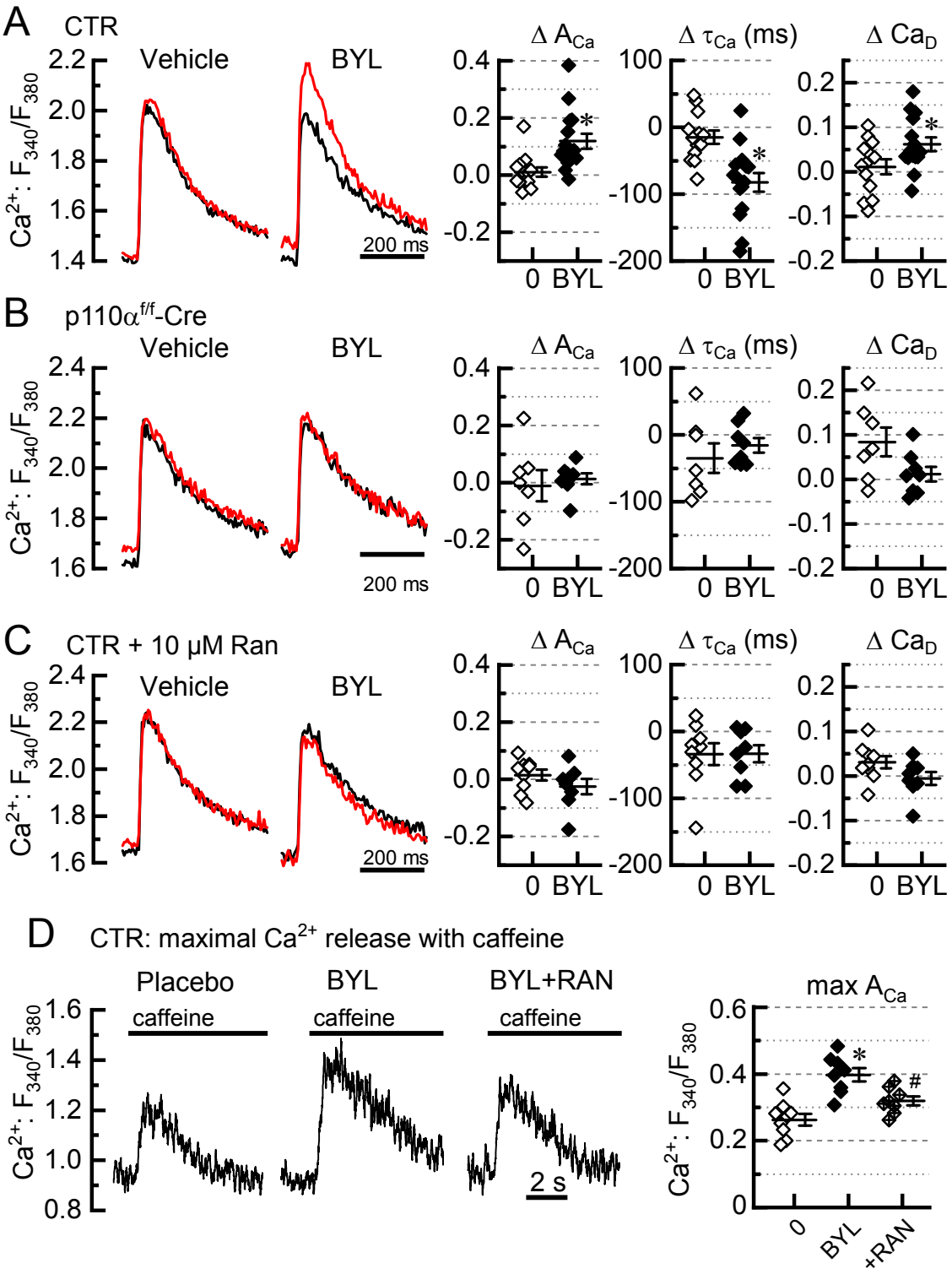

Figure 3. Effect of BYL on Ca^{2+} transients in isolated ventricular myocytes and ablation of the effect in PI3Kα-deficient myocytes and by pharmacological inhibition. **A**. BYL enhances Ca^{2+} transients in control myocytes (CTR); n = 13-15 myocytes per group (28 myocytes from 6 hearts). **B**. Lack of BYL effect on Ca^{2+} transients in PI3Kα-deficient myocytes (p110$\alpha^{f/f}$-Cre); n = 7-8 myocytes per group (15 myocytes from 4 hearts). **C**. Lack of BYL effect on Ca^{2+} transients in CTR myocytes in the presence of 10 μmol/l ranolazine (10 μM Ran); n = 8-9 myocytes per group (17 myocytes from 4 hearts). **D**. BYL enhances caffeine-induced Ca^{2+} release and ranolazine prevents effect of BYL. Representative releases are plotted on the left and absolute values of amplitudes of Ca^{2+} releases (max A_{Ca}) are plotted on the right; n = 8-9 (25 myocytes from 6 hearts). In **A**-**C**, myocytes were field stimulated at 1 Hz, and average time courses of Ca^{2+} transients are plotted on the left, and change from baseline (Δ) for Ca^{2+} transient amplitude (A_{Ca}), time constant of the decay (τ_{Ca}) and diastolic Ca (Ca_D) are plotted on the right. The time course before (black) and after (red) application of vehicle (0) or 100 nmol/l BYL. CTR is wild-type (WT) and p110$\alpha^{f/f}$ littermates of p110$\alpha^{f/f}$-Cre mice. ∗ $p < 0.05$ compared with vehicle; # $p < 0.05$ compared with BYL group.

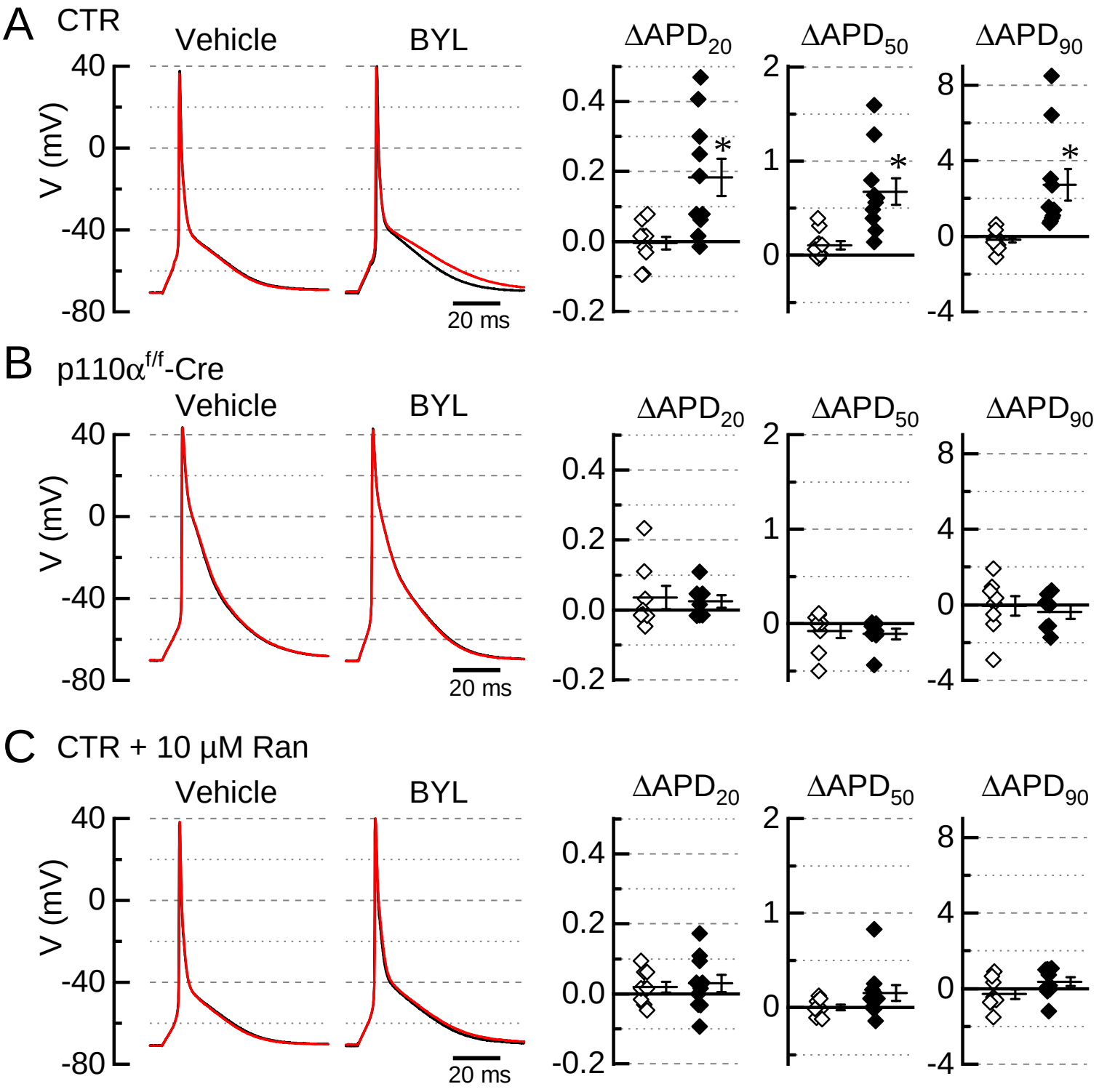

Figure 4. Effect of BYL on action potential in isolated ventricular myocytes and ablation of the effect in the PI3Kα-deficient model and by pharmacological intervention. **A**. BYL prolongs action potential in control (CTR) myocytes; n = 9-10 myocytes per group (19 myocytes from 4 hearts). **B**. Lack of BYL effect on action potential in PI3Kα-deficient myocytes (p110α$^{f/f}$-Cre); n = 7-8 myocytes per group (15 myocytes from 4 hearts). **C**. Lack of BYL effect on action potential in CTR myocytes in the presence of 10 µmol/l ranolazine (10 µM Ran); n = 9-10 myocytes per group (19 myocytes from 4 hearts). In all panels (**A**-**C**), representative action potentials are plotted on the left, and change in action potential duration (ΔAPD) at repolarization levels 20%, 50%, and 90% are plotted on the right. The action potentials before (black) and after (red) application of vehicle or 100 nmol/l BYL. CTR is wild-type (WT) and p110α$^{f/f}$ littermates of p110α$^{f/f}$-Cre mice. ∗ $p < 0.05$ compared with vehicle.

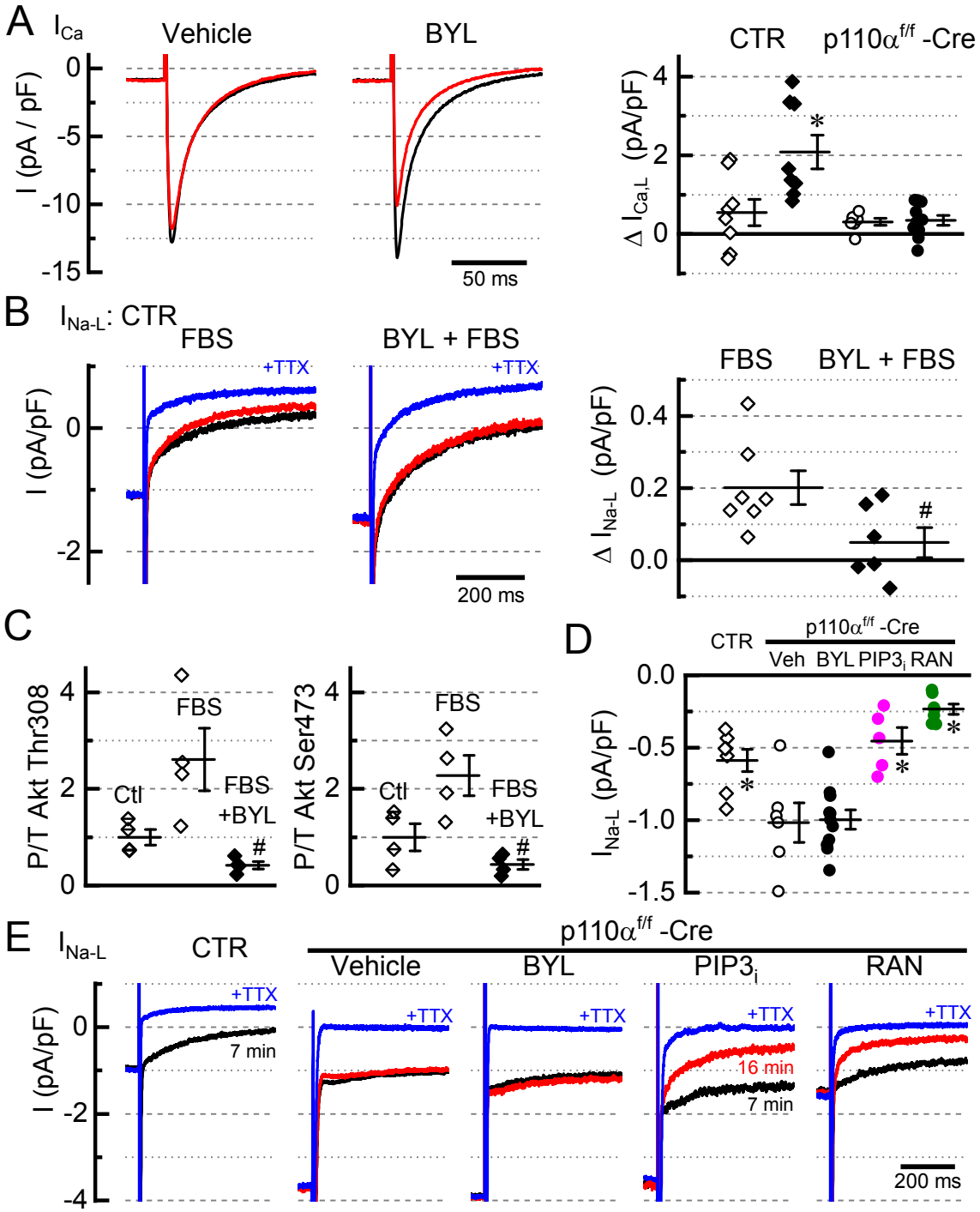

Figure 5. Effect of inhibition and activation of PI3Kα on ionic currents in isolated ventricular myocytes. **A**. Inhibition of L-type Ca^{2+} current ($I_{Ca,L}$) by 100 nmol/l BYL and lack of the effect of BYL in PI3Kα-deficient myocytes (p110α$^{f/f}$-Cre). Representative records of $I_{Ca,L}$ for control myocytes (CTR) in response to depolarization from –40 to 0 mV [before (black) and after (red) application of vehicle or 100 nmol/l BYL] (left). Change in amplitude of the peak $I_{Ca,L}$ ($\Delta I_{Ca,L}$) (right); n = 7-11 per group (34 mycytes; 8 hearts). **B**. Inhibition of late Na^+ current (I_{Na-L}) by FBS and diminished inhibition by FBS + 100 nmol/l BYL (FBS + BYL); n = 6-7 myocytes per group (13 myocytes; 4 hearts). **C**. Activation of PI3Kα by FBS and inhibition of PI3Kα by FBS + 100 nmol/l BYL (+BYL) in cultured isolated CTR cardiomyocytes. Ctl is control (no FBS, no BYL); n = 4 blots from 2 hearts. **D**. Current densities of I_{Na-L} in normal (CTR) and PI3Kα-deficient myocytes (p110α$^{f/f}$-Cre) for vehicle (Veh), 100 nmol/l BYL (BYL), 1 μmol/l intracellular PIP3 (PIP3$_i$), and 10 μmol/l ranolazine (RAN); n = 5-11 myocytes per group (36 myocytes; 9 hearts). **E**. Representative traces of late Na^+ current (I_{Na-L}) for conditions described in *D*; times listed are post-dialysis times. In **D** and **E**, late Na^+ current (I_{Na-L}) was invoked in response to 500-ms depolarization from –120 to –40 mV and was measured as TTX-sensitive current at the end of depolarization. Representative records: current before intervention (black), after intervention (red), and background (blue, +5 μmol/l TTX). FBS, mixture of 0.2% fetal bovine serum with 50 U/L insulin; CTR, WT and p110α$^{f/f}$ littermates. ∗ $p < 0.05$ compared with vehicle; # $p < 0.05$ compared with FBS.

Zhabyeyev P. et al. (2019)

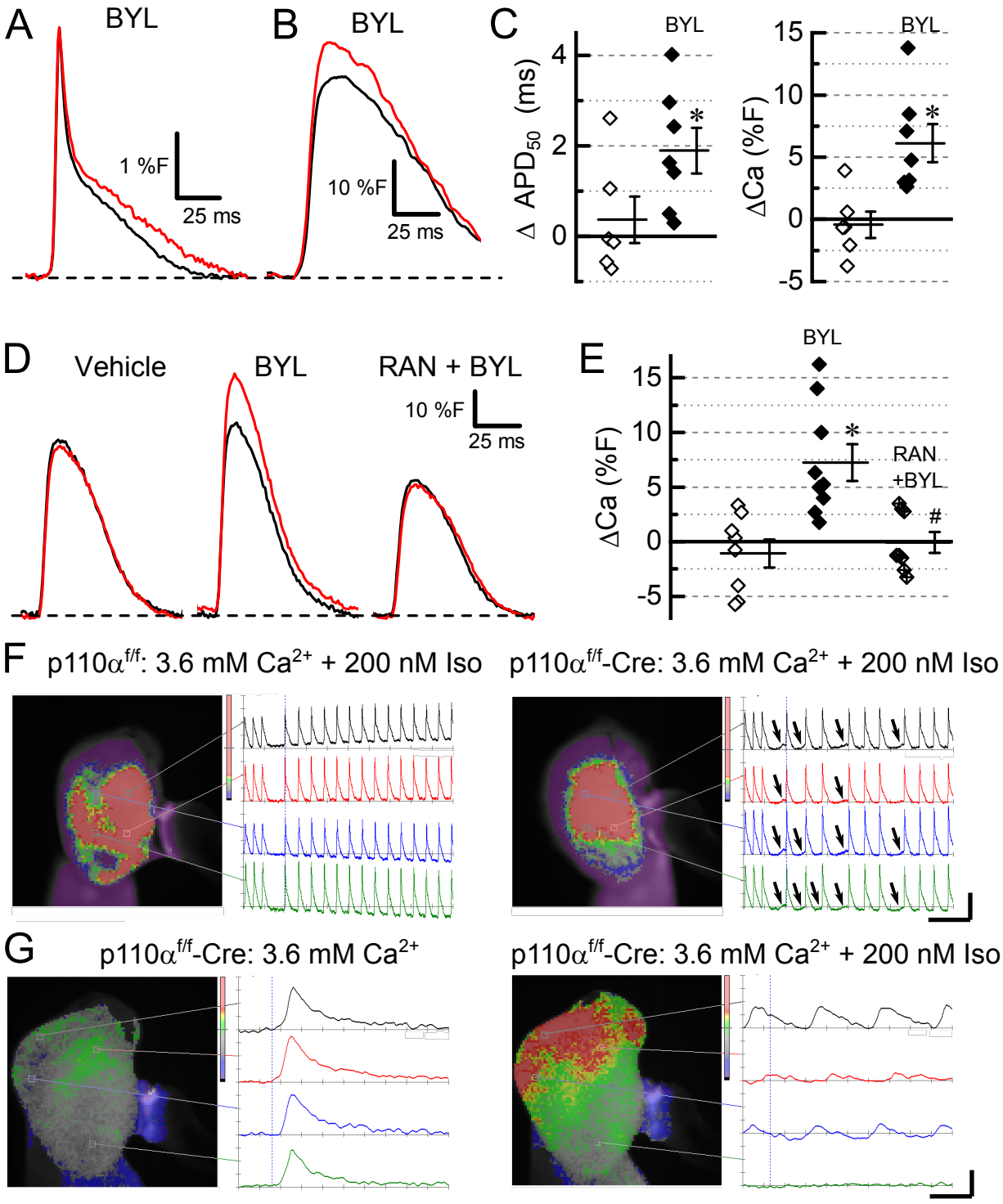

Figure 6. BYL prolongs action potential, enhances Ca^{2+} release, and trigger arrhythmias in *ex vivo* hearts. **A**. Representative action potentials before (black) and after (red) application of 100 nmol/l BYL, paced at 6 Hz. **B**. Representative traces of Ca^{2+} release before (black) and after (red) application of 100 nmol/l BYL, paced at 6 Hz. **C**. Change in the action potential duration at 50% repolarization (APD_{50}) and in the amplitude of Ca^{2+} transient due to application of vehicle or BYL, paced at 6 Hz; n = 6-7. **D**. Representative traces of Ca^{2+} transients before (black) and after (red) application of vehicle, 100 nmol/l BYL (BYL), or 10 µmol/l RAN + 100 nmol/l BYL (RAN + BYL) in the presence of 200 nmol/l of isoproterenol, paced at 12 Hz; n = 8-9. **E**. Change in the amplitude of Ca^{2+} transients in the presence of 200 nmol/l of isoproterenol, paced at 12 Hz, in response to application of vehicle, 100 nmol/l BYL (BYL), or 10 µmol/l RAN + 100 nmol/l BYL (RAN + BYL), paced at 12 Hz. **F**. Representative frame and traces for $p110\alpha^{f/f}$ littermate ($p110\alpha^{f/f}$) (left) and PI3Kα-deficient hearts ($p110\alpha^{f/f}$-Cre) (right) in the presence of 3.6 mmol/l Ca^{2+} + 200 nM isoproterenol (Iso) in response to burst pacing for 1.5 s at 12 Hz. Instances of delayed afterdepolarizations are marked with arrows; calibration bar 5 %F and 400 ms. **G**. An instance of ventricular fibrillation in PI3Kα-deficient heart ($p110\alpha^{f/f}$-Cre) heart in response to application of 200 nmol/l isoproterenol (Iso) in the presence of 3.6 mmol/l Ca^{2+}; calibration bar 2 %F and 20 ms. ∗ $p < 0.05$ compared with vehicle. # $p < 0.05$ compared with BYL.

Zhabyeyev P. et al. (2019)

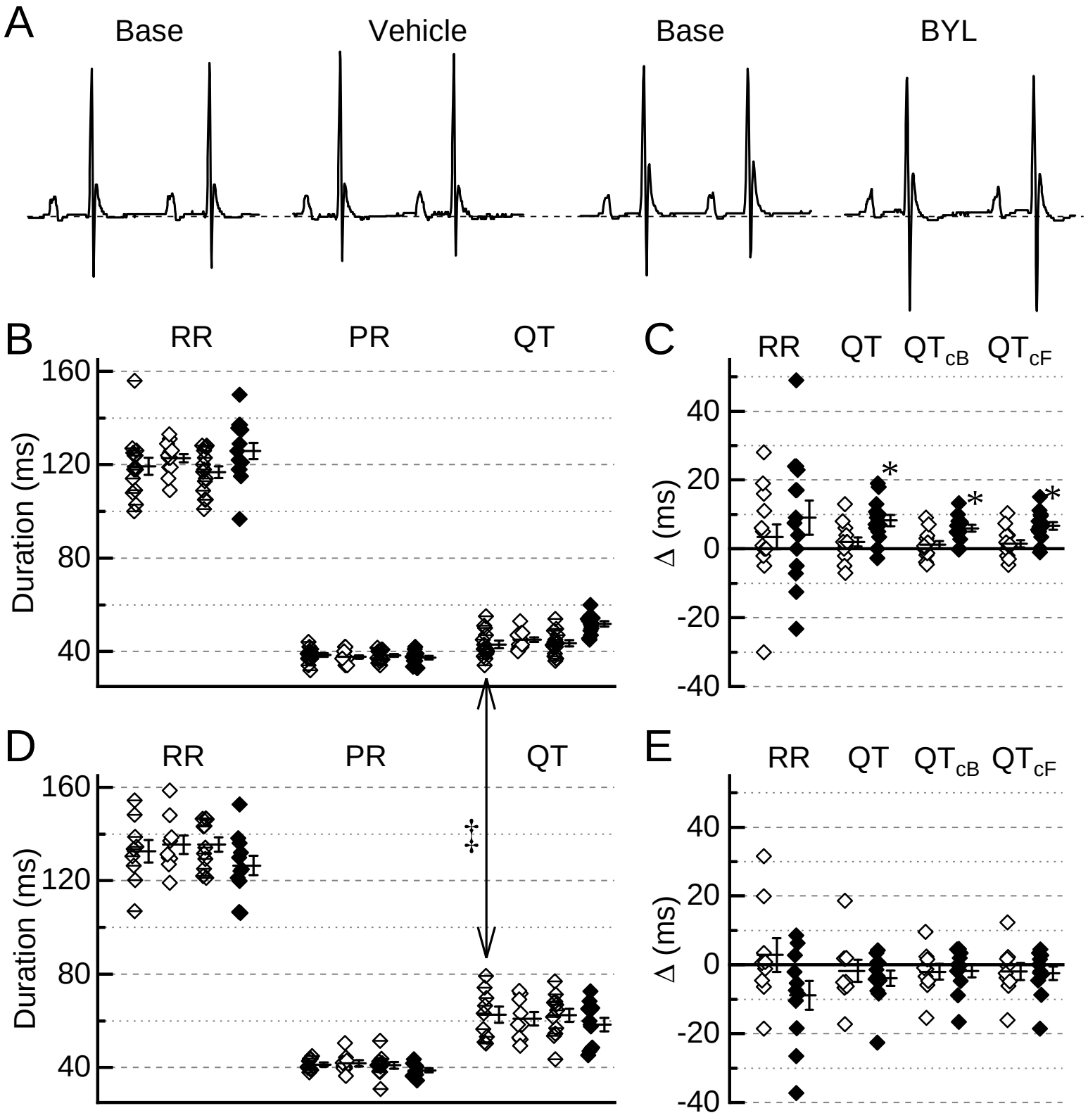

Figure 7. BYL prolongs QT interval in a PI3Kα-dependent manner. **A**. Representative pairs of electrocardiographic (ECG) traces for WT and p110$\alpha^{f/f}$ littermate mice (CTR): before (base) and after administration of the vehicle (left) and before (base) and after administration of BYL (right). **B**. Interval duration for RR, PR, and QT intervals for CTR mice. **C**. Change in the duration of RR, QT, QT_{cB} (Bazett correction), and QT_{cF} (Fridericia correction) calculated from values in B. **D**. Interval duration for RR, PR, and QT intervals for PI3Kα-deficient mice (p110$\alpha^{f/f}$-Cre). **E**. Change in the duration of RR, QT, QT_{cB} (Bazett correction), and QT_{cF} (Fridericia correction) calculated from values in D. ∗ $p < 0.05$ compared with vehicle, ‡ $p < 0.05$ for comparison between pooled baselines.

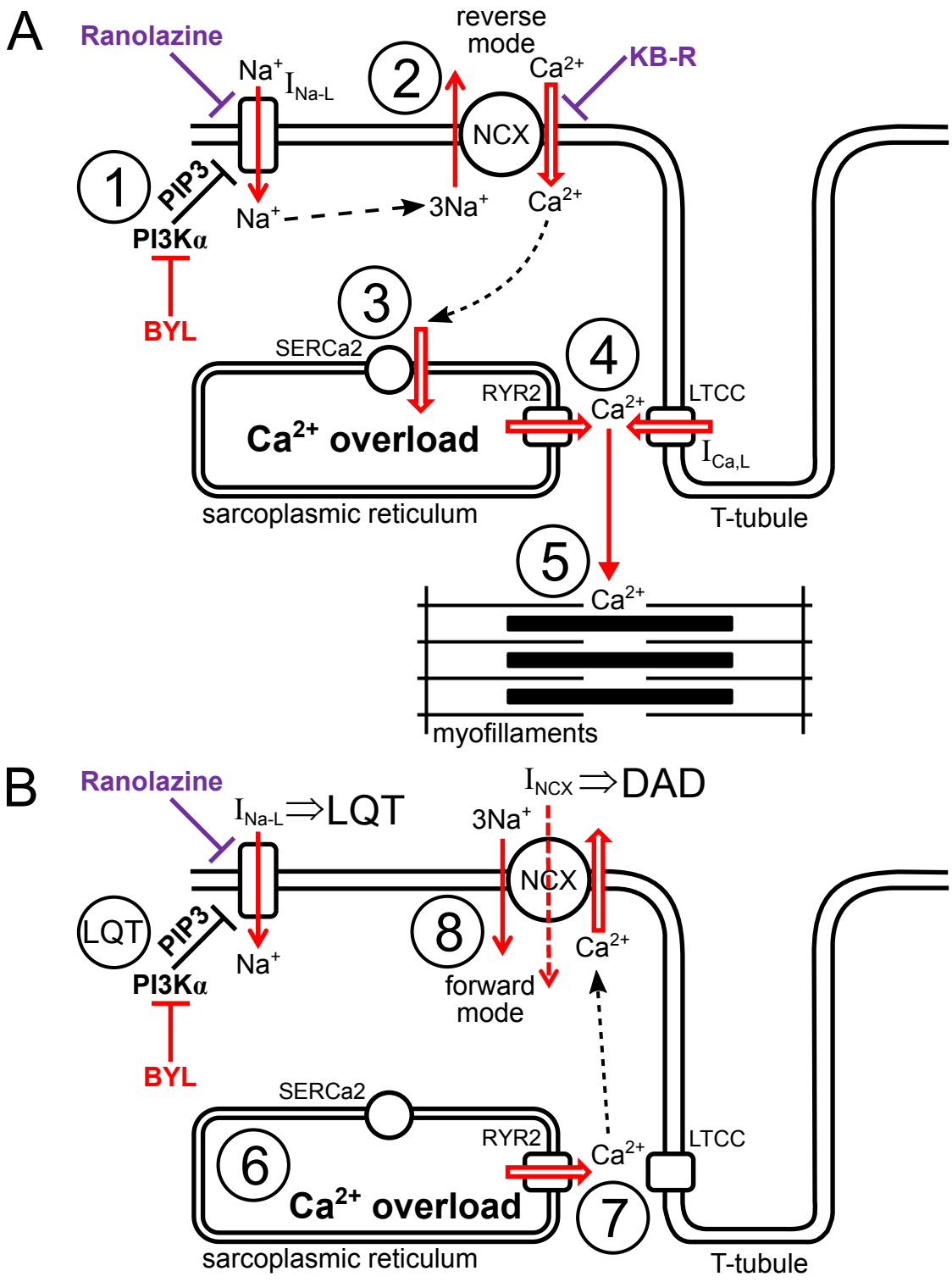

Figure 8. PI3Kα, Ca^{2+} cycling, contractility, and arrhythmias. **A**. Enhanced Ca^{2+} release and contractility due to PI3Kα inhibition. (1) PIP3 produced by PI3Kα suppresses activation of late Na^+ current ($I_{Na\text{-}L}$). Once PI3Kα is inhibited by BYL, lack of PIP3 activates (dis-inhibits) $I_{Na\text{-}L}$, and additional Na^+ flows into the cell during action potential. (2) Additional Na^+ is exchanged for additional intracellular Ca^{2+} *via* reverse mode of Na^+-Ca^{2+} exchanger (NCX). (3) Additional Ca^{2+} is re-uptaken into sarcoplasmic reticulum (SR) *via* sarco-endoplasmic reticulum Ca^{2+}-ATPase (SERCa2) increasing Ca^{2+} load of the SR. (4) Increased Ca^{2+} load leads to larger Ca^{2+} release *via* Ca^{2+} release channels (RYR2) and, in turn, (5) enhanced contractility. Ca^{2+} build up in the SR can be interrupted at step (1) by ranolazine ($I_{Na\text{-}L}$ blocker) or at step (2) by KB-R (reverse-mode NCX blocker). **B**. Pro-arrhythmic effects of PI3Kα inhibition. (LQT) Inhibition of PI3Kα (*e.g.*, BYL) will activates (disinhibits) $I_{Na\text{-}L}$, a depolarizing current, that may directly prolong action potential. Pro-arrhythmic action due to (6) Ca^{2+} overload (during β-adrenergic stimulation and PI3Kα inhibition) is initiated by (7) spontaneous Ca^{2+} release *via* RYR2. Excess of Ca^{2+} is exchanged for Na^+ (8) generating net inward (depolarizing current) current *via* NCX (I_{NCX}; 3 Na^+ – 1 Ca^{2+} = +1 net transfer into the cell). The depolarizing I_{NCX} produces membrane depolarization (delayed afterdepolarization, DAD) that may result in triggered activity.

Zhabyeyev P. et al. (2019)

	DAD count			
	5 min	7 min	9 min	Total
CTR	0	0	0	0
	0	0	0	0
	0	0	0	0
	0	0	0	0
	1	1	0	2
	0	0	0	0
p110$\alpha^{f/f}$-Cre	0	0	0	0
	3	3	4	10
	3	3	3	3
	0	0	1	1
	1	0	0	1
	4	4	4	12
	4	4	3	11

Table S1. Delayed afterdepolarization (DAD) count for normal (CTR) and PI3Kα-deficient (p110$\alpha^{f/f}$-Cre) hearts subjected to arrhythmic protocol. Hearts were exposed to 3.6 mmol/l Ca^{2+} and 200 nmol/l isoproterenol and 1.5 s of 12-Hz pacing. DAD were counted 2 s after pacing burst. Independent sample Kurskal-Wallis test suggest mean rank difference between the groups ($p = 0.02$)

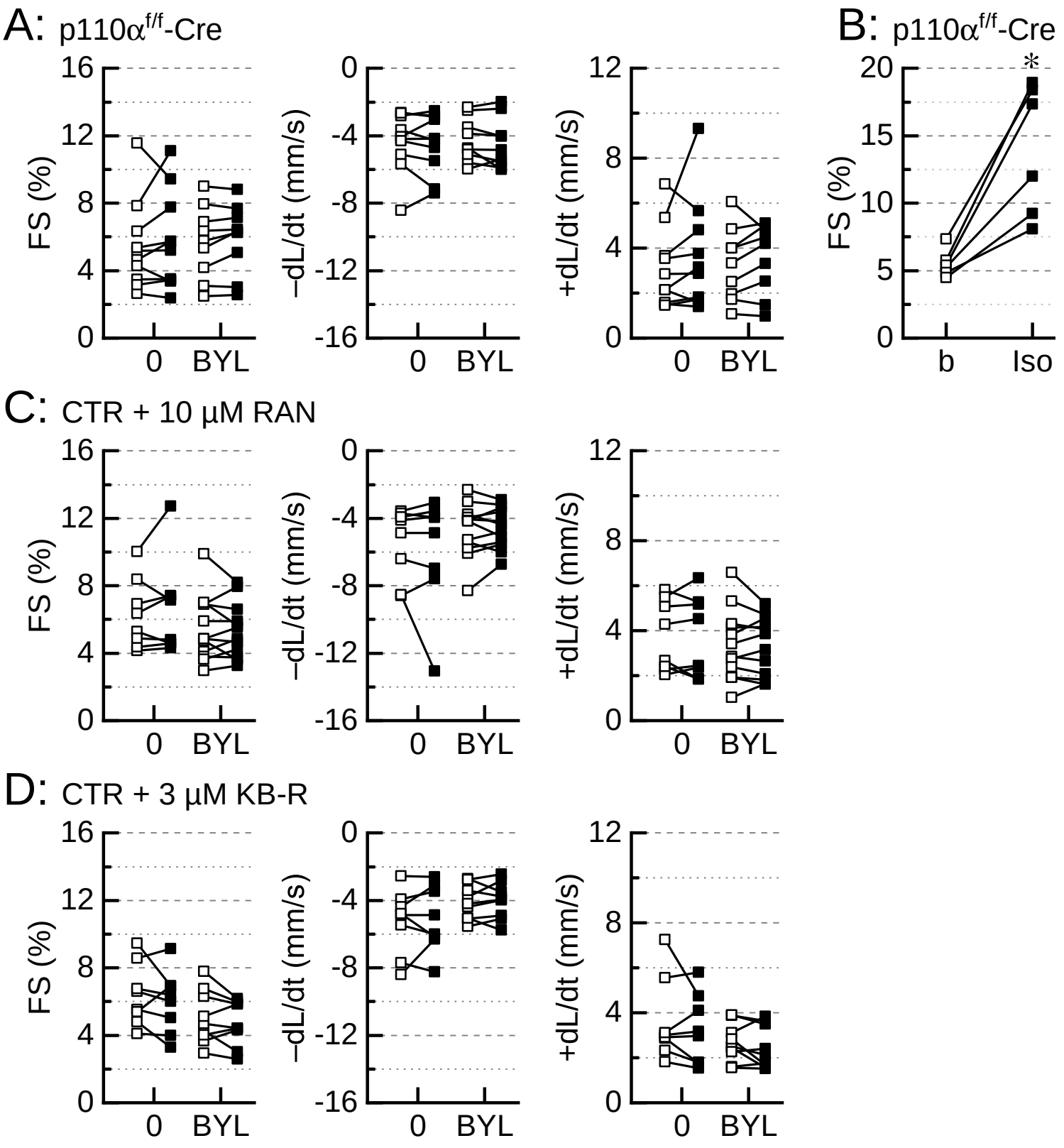

Figure S1. Time series of absolute values for fractional shortening (FS), rate of contraction (–dL/dt$_{max}$, C), and rate of relaxation (+dL/dt$_{max}$, R). **A**. Lack of the effect of BYL on contractility in PI3Kα-deficient myocytes (p110α$^{f/f}$-Cre); n = 9-10 myocytes per group (19 myocytes from 4 hearts). **B**. Effect of 1 µmol isoproterenol on fractional shortening (FS) in PI3Kα-deficient myocytes (p110α$^{f/f}$-Cre); n = 6 myocytes from 1 heart (paired t-test comparing baseline (b) to 1 µmol/l Iso). **C**. Lack of the effect of BYL on contractility in the presence of 10 µmol/l ranolazine (Ran); n = 8-12 myocytes per group (20 myocytes from 4 hearts). **D**. Lack of the effect of BYL on contractility in the presence of 3 µmol/l KB-R7943 (KB-R); n = 8-9 myocytes per group (17 myocytes from 4 hearts). 0, vehicle; BYL, 100 nM BYL; field stimulation at 1 Hz.

Zhabyeyev P. et al. (2019)

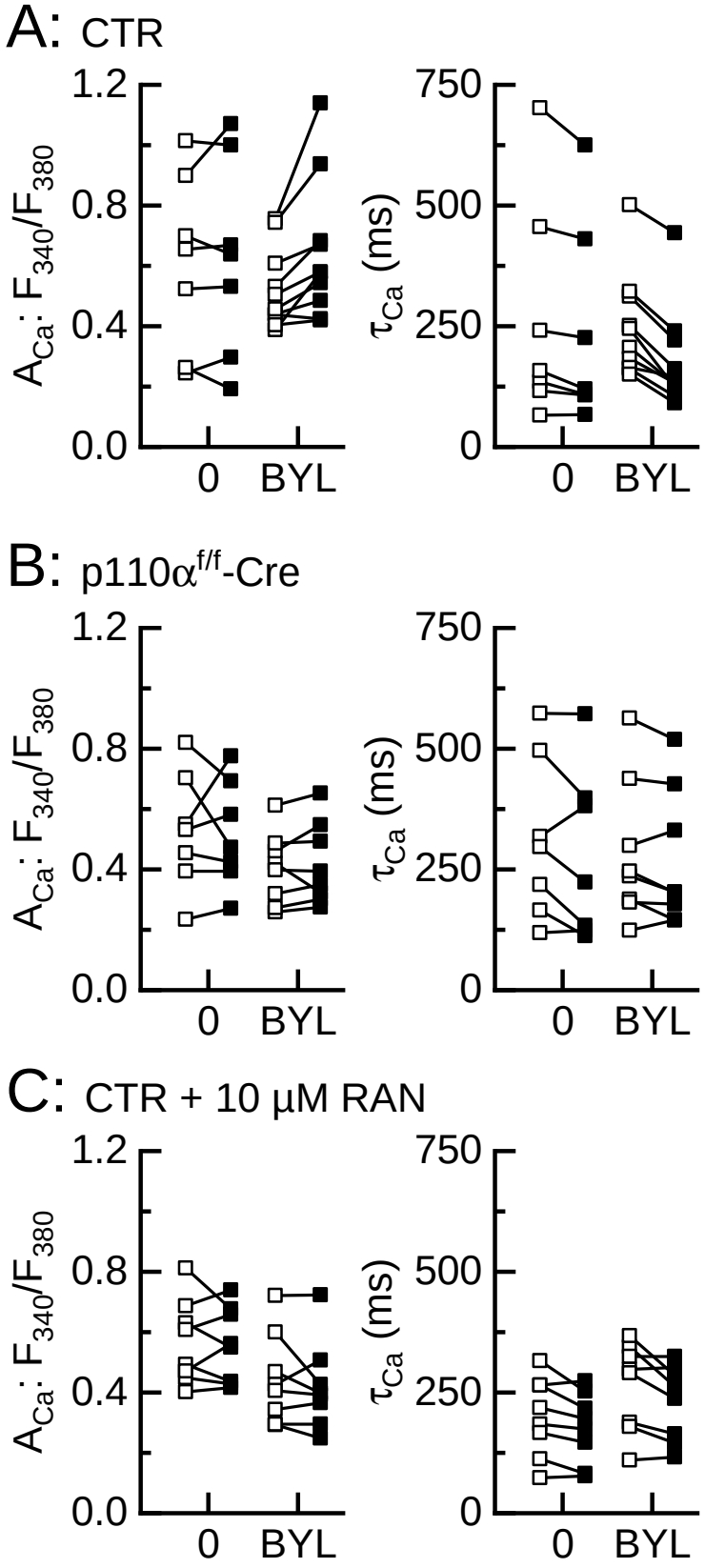

Figure S2. Absolute values for amplitude of Ca^{2+} transient and time constant of Ca^{2+} transient (τ_{Ca}) before (open) and after (filled) of application of vehicle (0) or BYL. **A**. Effect of BYL on Ca^{2+} transient in control myocytes (CTR); n = 13-15 myocytes per group (28 myocytes from 6 hearts). **B**. Lack of the effect of BYL on Ca^{2+} transient in PI3Kα-deficient myocytes (p110α$^{f/f}$-Cre); n = 7-8 myocytes per group (15 myocytes from 4 hearts). **C**. Lack of the effect of BYL on Ca^{2+} transient in the presence of 10 µmol/l ranolazine (Ran). In all panels (**A-C**), Ca^{2+} transients were measured with Ca^{2+}-sensitive dye FURA-2 in myocyte paced at 1 Hz with field stimulation; for statistical analysis see Figure 3.

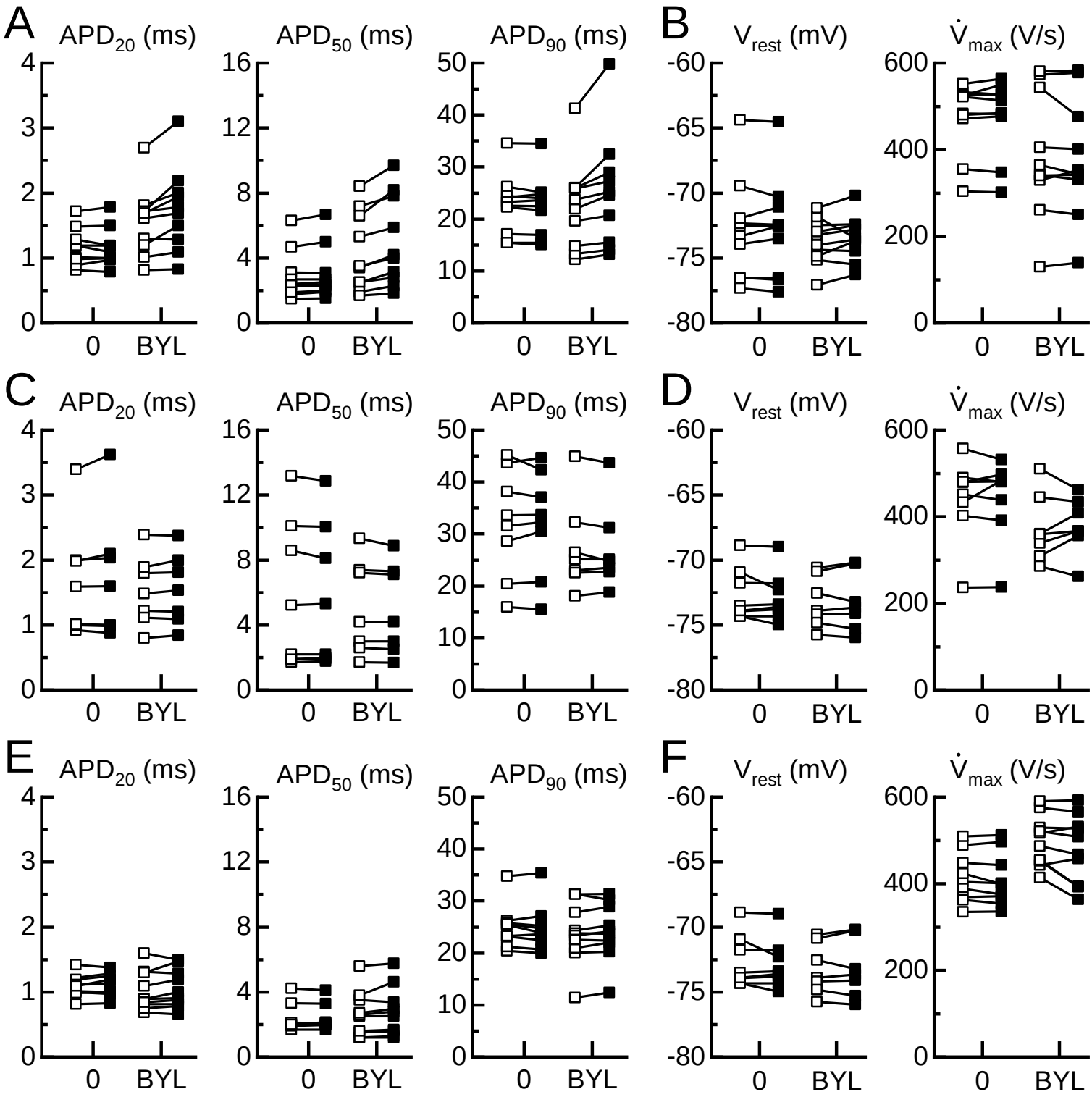

Figure S3. Absolute values for action potential parameters before and after application of vehicle (0) or BYL. **A**. Action potential durations (APDs) in control myocytes (CTR) exposed to vehicle (0) or BYL. **B**. Resting membrane potential V_{rest} and maximal upstroke velocity ($\dot{V}_{max}$) in control myocytes (CTR) exposed to vehicle (0) or BYL. **A**-**B**: n = 9-10 myocytes per group (19 myocytes from 4 hearts); for statistical analysis see Figure 4A. **C**. Action potential durations (APDs) in PI3Kα-deficient myocytes (p110$\alpha^{f/f}$-Cre) exposed to vehicle (0) or BYL. **D**. Resting membrane potential V_{rest} and maximal upstroke velocity ($\dot{V}_{max}$) in PI3Kα-deficient myocytes (p110$\alpha^{f/f}$-Cre) exposed to vehicle (0) or BYL. **C**-**D**: n = 7-8 myocytes per group (15 myocytes from 4 hearts). **E**. Action potential durations (APDs) in control myocytes (CTR) treated with 10 µmol/l ranolazine (RAN) exposed to vehicle (0) or BYL. **F**. Resting membrane potential V_{rest} and maximal upstroke velocity ($\dot{V}_{max}$) in control myocytes (CTR) exposed to vehicle (0) or BYL. **E**-**F**: n = 9-10 myocytes per group (19 myocytes from 4 hearts).

Zhabyeyev P. et al. (2019)

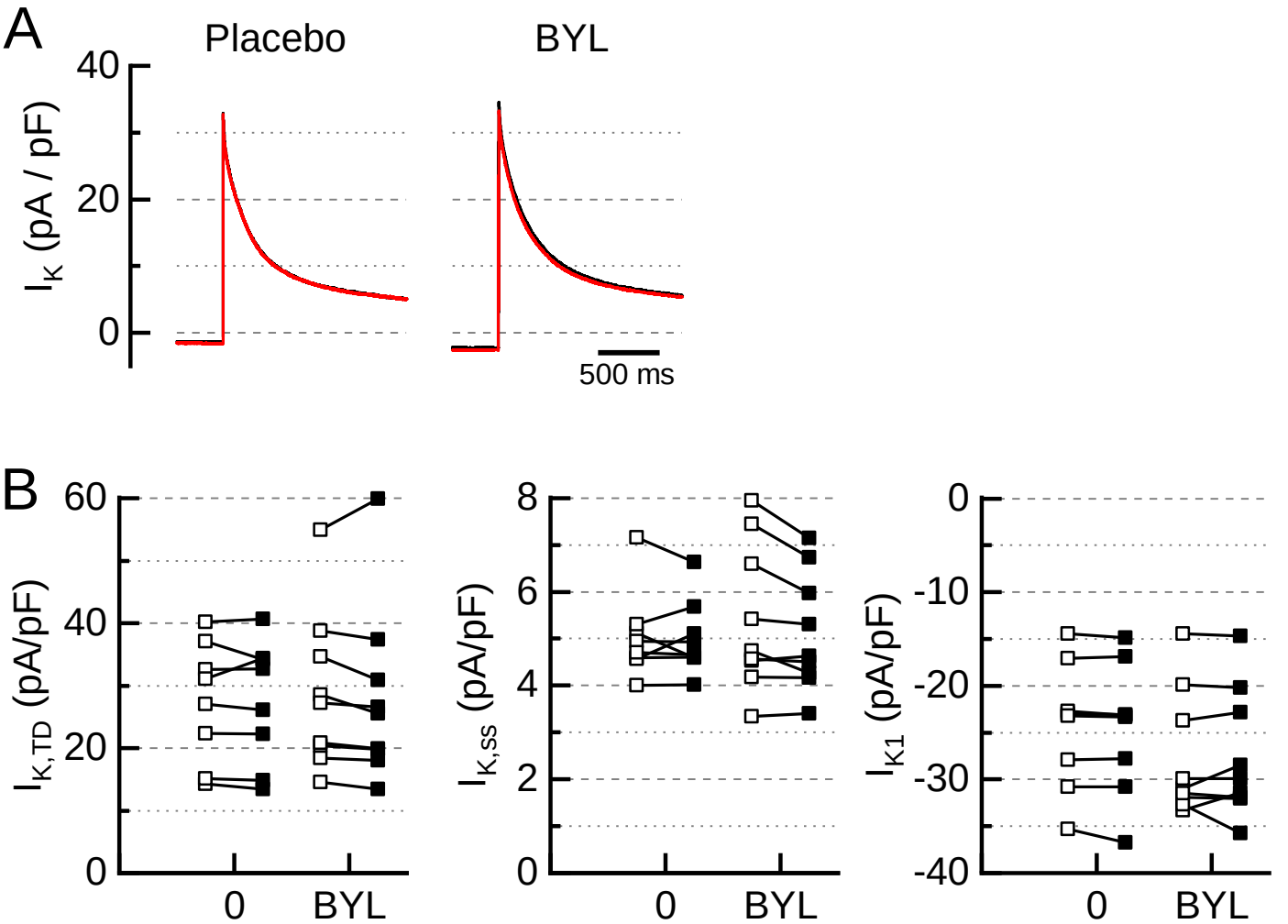

Figure S4. BYL has no effect on K^+ currents in control myocytes. **A**. Average traces in response to 500-ms depolarization from –85 to +20 mV. Before (black) and after (red) application of vehicle or BYL). **B**. Absolute values of current densities for $I_{K,TD}$, $I_{K,ss}$, and I_{K1} before and after application of vehicle (0) or BYL.

Zhabyeyev P. et al. (2019)

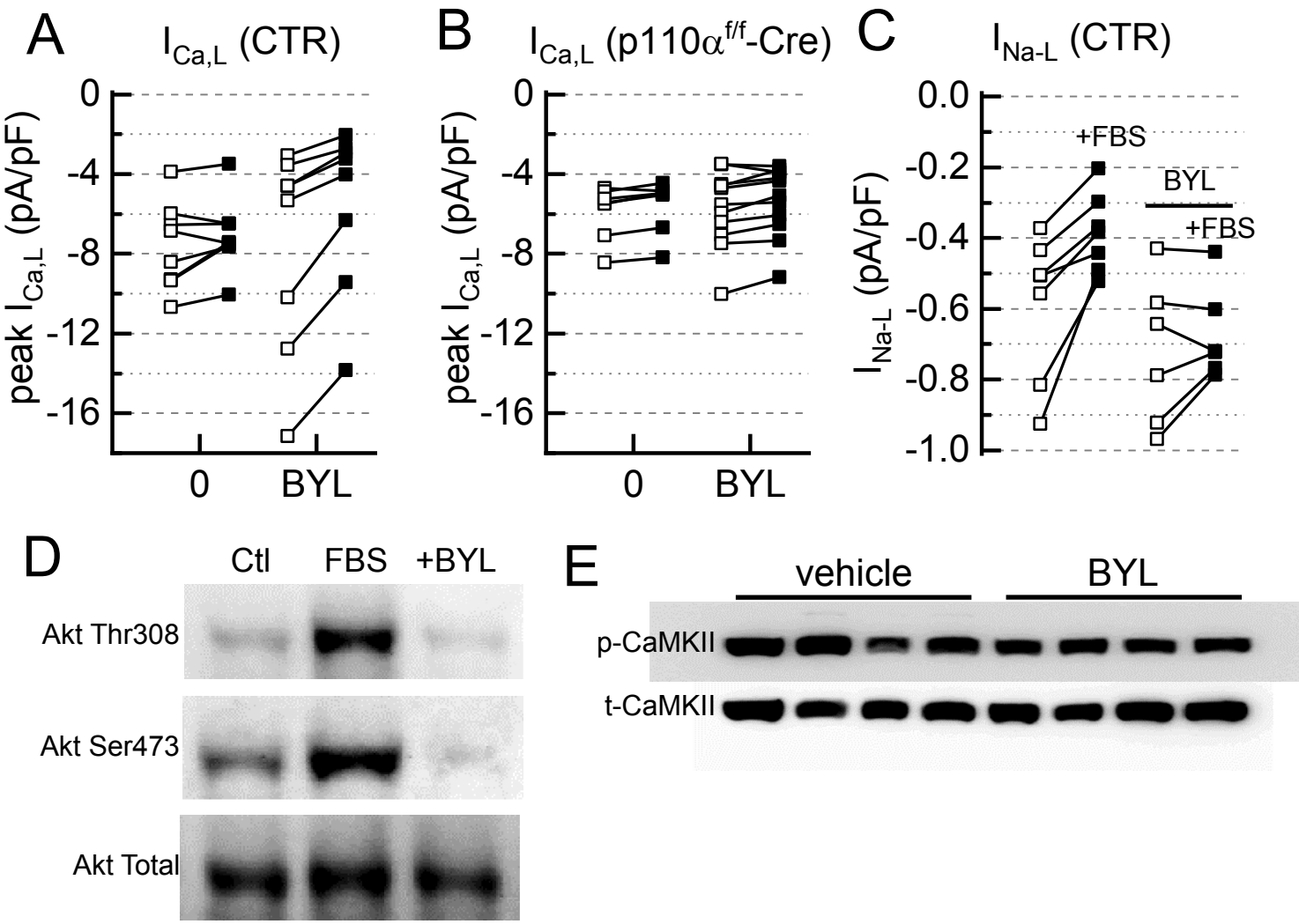

Figure S5. Changes in L-type Ca^{2+} current ($I_{Ca,L}$), late Na^+ current (I_{Na-L}), and phosphorilation of Ca^{2+}/calmodulin-dependent protein kinase II (CaMKII) in response to BYL. **A**. Current densities of peak $I_{Ca,L}$ before and after application of vehicle (0) or BYL in controlmyocytes (CTR) in response to depolarizations from –40 to 0 mV. $I_{Ca,L}$ is defined as 3-μM nisoldipine-sensitive current; n = 8 myocytes per group (16 myocytes; 4 hearts total). **B**. Current densities of peak $I_{Ca,L}$ before and after application of vehicle (0) or BYL in PI3Kα-deficient myocytes (p110α$^{f/f}$-Cre) (the same protocol as in *A*); n = 7-11 myocytes per group (18 myocytes; 5 hearts total. **C**. Current densities of I_{Na-L} before and after application of 0.2% fetal bovine serum with 50 U/l insulin (+FBS) in the absence and in the presence of 100 nmol/l BYL. I_{Na-L} was elicited in response to depolarization from –120 to –40 mV and defined as 5-μM tetrodotoxin-sensitive current. **D**. Representative blots of phosphorylation levels of Akt Thr308 and Akt S473 in cultured CTR cardiomyocytes in response to mixture of 0.2% fetal bovine serum and 50 U/l insulin (FBS) and to FBS + 100 nmol/l BYL (+BYL); Ctl, no FBS or BYL was added. **E**. CaMKII phosphorylation levels in the hearts from animals treated with vehicle or BYL (30 mg/kg for 4 days).

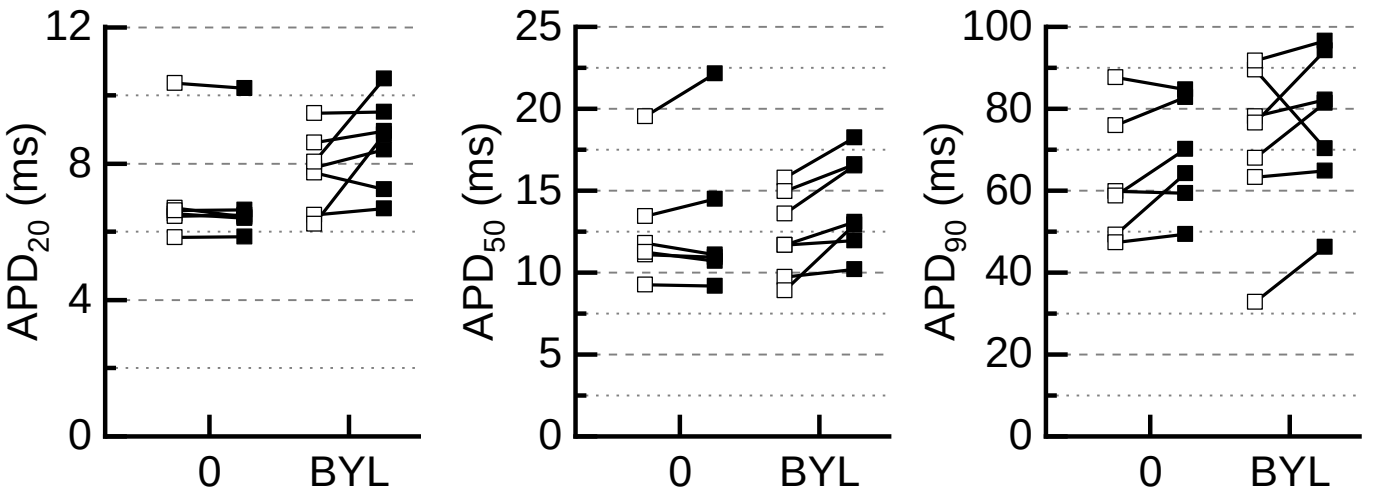

Figure S6. Effect of BYL on action potential duration (APD) in *ex vivo* hearts. APD at 20% repolarization (APD_{20}), APD at 50% repolarization (APD_{50}), and APD at 90% repolarization (APD_{90}) before and after application of vehicle (0) and BYL; paced at 6 Hz; n = 6-7.

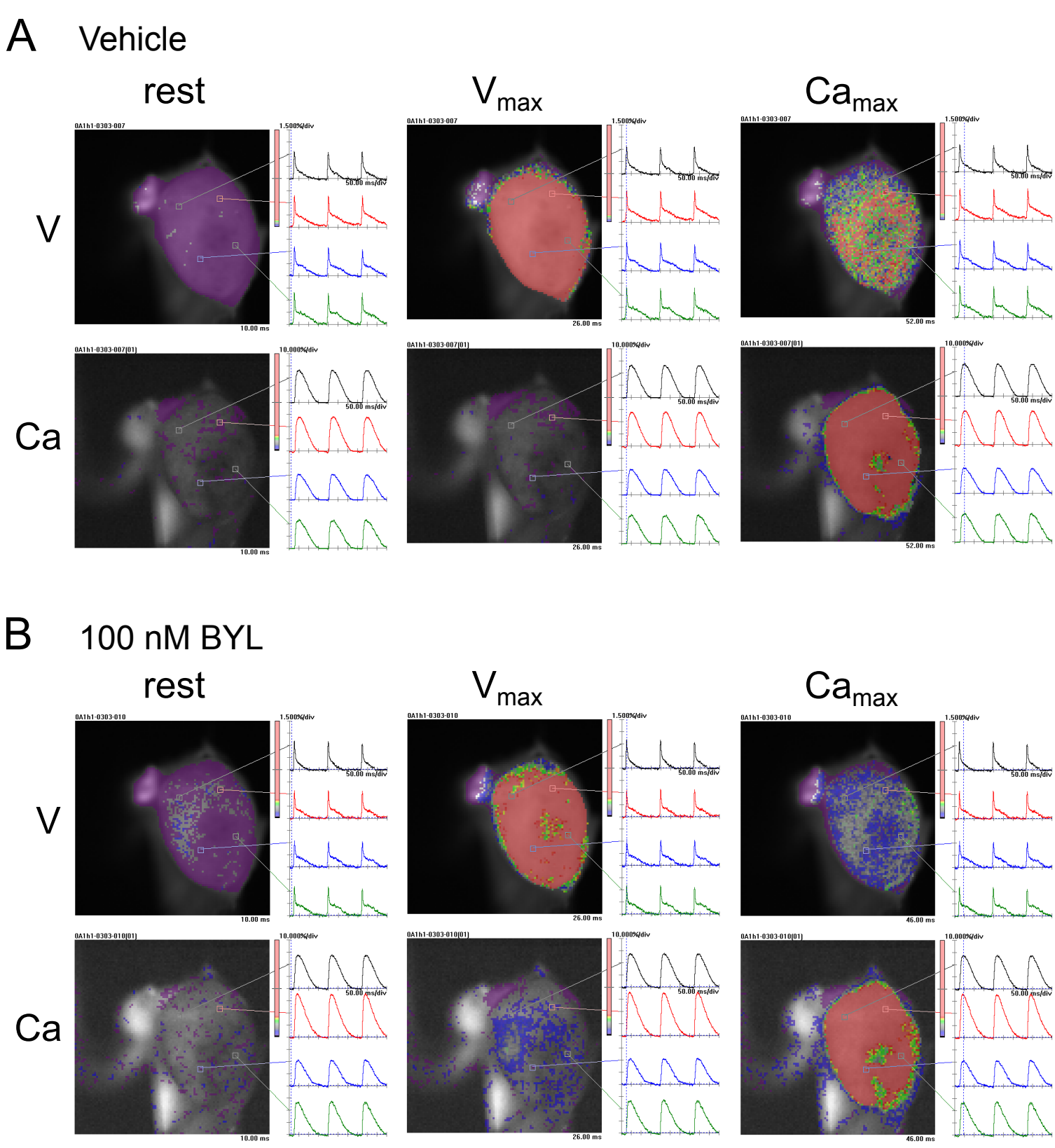

Figure S7. Examples of heart images with voltage and Ca^{2+} sensitive dyes. **A**. Vehicle (DMSO) treatment. **B**. BYL (100 nmol/l) treatment. **A** and **B**. Images of hearts with voltage (V) sensetive (RH237, top row) and Ca^{2+} sensitve (Rhod-2AM, bottom row) dyes at the time points marked on adjacent time plot and corresponded to rest, maximal voltage signal (V_{max}), and maximal Ca^{2+} signal (Ca_{max}).